

Lanthanide Metal-Organic Frameworks and Hierarchical Porous Zeolitic Imidazolate Frameworks

Synthesis, Properties, and Applications

Hani Nasser Abdelhamid

Academic dissertation for the Degree of Doctor of Philosophy in Inorganic Chemistry at Stockholm University to be publicly defended on Thursday 12 October 2017 at 13.00 in Magnélisalen, Kemiska övningslaboratoriet, Svante Arrhenius väg 16 B.

Abstract

This thesis presents the synthesis, properties, and applications of two important classes of metal-organic frameworks (MOFs); lanthanide MOFs and hierarchical porous zeolitic imidazolate frameworks (ZIFs). The materials have been characterized using a wide range of techniques including diffraction, imaging, various spectroscopic techniques, gas sorption, dynamical light scattering (DLS) and thermogravimetric analysis (TGA).

In Chapter 1, the unique features of MOFs and ZIFs as well as their potential applications are summarized. In Chapter 2, different characterization techniques are presented.

Chapter 3 describes a family of new isoreticular lanthanide MOFs synthesized using tri-topic linkers of different sizes, H_3L1-H_3L4 , denoted SUMOF-7I-IV (Ln) (SU; Stockholm University, $Ln = La, Ce, Pr, Nd, Sm, Eu$ and Gd , Paper I). The SUMOF-7I-III (Ln) contain permanent pores and exhibit exceptionally high thermal and chemical stability. The luminescence properties of SUMOF-7II are reported (Paper II). The influences of Ln ions and the tri-topic linkers as well as solvent molecules on the luminescence properties are investigated. Furthermore, the potential of SUMOF-7II (La) for selective sensing of Fe (III) ions and the amino acid tryptophan is demonstrated (Paper III).

Chapter 4 presents a simple, fast and scalable approach for the synthesis of hierarchical porous zeolitic imidazolate framework ZIF-8 and ZIF-67 using triethylamine (TEA)-assisted approach (Paper IV). Organic dye molecules and proteins are encapsulated directly into the ZIFs using the one-pot method. The photophysical properties of the dyes are improved through the encapsulation into ZIF-8 nanoparticles (Paper IV). The porosity and surface area of the ZIF materials can be tuned using the different amounts of dye or TEA. To further simplify the synthesis of hierarchical porous ZIF-8, a template-free approach is presented using sodium hydroxide, which at low concentrations induces the formation of zinc hydroxide nitrate nanosheets that serve as in situ sacrificial templates (Chapter 5, Paper V). A 2D leaf-like ZIF (ZIF-L) is also obtained using the method. The hierarchical porous ZIF-8 and ZIF-L show good performance for CO_2 sorption.

Keywords: Metal-organic frameworks, Zeolitic imidazolate frameworks, Lanthanide MOFs, Hierarchical porous ZIFs.

Stockholm 2017

<http://urn.kb.se/resolve?urn=urn:nbn:se:su:diva-146398>

ISBN 978-91-7649-972-6
ISBN 978-91-7649-973-3

Department of Materials and Environmental Chemistry (MMK)

Stockholm University, 106 91 Stockholm



Stockholm
University

LANTHANIDE METAL-ORGANIC FRAMEWORKS AND
HIERARCHICAL POROUS ZEOLITIC IMIDAZOLATE FRAMEWORKS

Hani Nasser Abdelhamid



Lanthanide Metal-Organic Frameworks and Hierarchical Porous Zeolitic Imidazolate Frameworks

Synthesis, Properties, and Applications

Hani Nasser Abdelhamid

Doctoral Thesis 2017

Department of Materials and Environmental Chemistry
Arrhenius Laboratory, Stockholm University
S-106 91 Stockholm, Sweden

Faculty Opponent:

Prof. Banglin Chen
Department of Chemistry
University of Texas at San Antonio, USA

Evaluation committee:

Professor. Aji Mathew
Department of Materials and Environmental Chemistry
Stockholm University, Sweden

Associate Professor. Eszter Borbas
Department of Chemistry
Uppsala University, Sweden

Professor. Muhammet S. Toprak
School of Engineering Sciences
Royal Institute of Technology, Sweden

Substitute:

Associate Professor. Timofei Privalov
Department of Organic Chemistry
Stockholm University

Cover image shows the structure of SUMOF-7II, antenna effects and synthesis of hierarchical porous ZIF-8 from ZnO and Zn hydroxyl nanosheets.

©Hani Nasser Abdelhamid, Stockholm University 2017

ISBN tryckt 978-91-7649-972-6
ISBN PDF 978-91-7649-973-3

Printed by Universitetsservice US-AB, Stockholm 2017
Distributor: Department of Materials and Environmental Chemistry, Stockholm University

Although my father passed away unexpectedly when I was in my PhD study, I still feel his impact every day.

Khem or Chem refers to the Egyptian word for "black", Alchemy is the "Egyptian art".
Oxford English Dictionary

Abstract

This thesis presents the synthesis, properties, and applications of two important classes of metal-organic frameworks (MOFs); lanthanide MOFs and hierarchical porous zeolitic imidazolate frameworks (ZIFs). The materials have been characterized using a wide range of techniques including diffraction, imaging, various spectroscopic techniques, gas sorption, dynamic light scattering (DLS) and thermogravimetric analysis (TGA).

In Chapter 1, the unique features of MOFs and ZIFs as well as their potential applications are summarized. In Chapter 2, different characterization techniques are presented.

Chapter 3 describes a family of new isoreticular lanthanide MOFs synthesized using tri-topic linkers of different sizes, H_3L1-H_3L4 , denoted SUMOF-7I-IV (Ln) ($Ln = La, Ce, Pr, Nd, Sm, Eu$ and Gd , Paper I). The SUMOF-7I-III (Ln) contains permanent pores and exhibits exceptionally high thermal and chemical stability. The luminescence properties of SUMOF-7IIs are reported (Paper II). The influences of Ln ions and the tri-topic linkers as well as solvent molecules on the luminescence properties are investigated. Furthermore, the potential of SUMOF-7II (La) for selective sensing of Fe (III) ions and the amino acid tryptophan is demonstrated (Paper III).

Chapter 4 presents a simple, fast, and scalable approach for the synthesis of hierarchical porous zeolitic imidazolate framework ZIF-8 and ZIF-67 using triethylamine (TEA)-assisted approach (Paper IV). Organic dye molecules and proteins are encapsulated directly into the ZIFs using one-pot method. The photophysical properties of the dyes are improved through the encapsulation into ZIF-8 nanoparticles (Paper IV). The porosity and surface area of the ZIF materials can be tuned using the different amounts of dye, or TEA. To further simplify the synthesis of hierarchical porous ZIF-8, a template-free approach is presented using sodium hydroxide, which at low concentrations induces the formation of zinc hydroxide nitrate nanosheets that serve as *in situ* sacrificial templates (Chapter 5, Paper V). A 2D leaf-like ZIF (ZIF-L) is also obtained using this method. The hierarchical porous ZIF-8 and ZIF-L show good performance for CO_2 sorption.

Keywords: Metal-organic frameworks; Zeolitic imidazolate frameworks; Lanthanide MOFs; Hierarchical porous ZIFs.

Abstrakt

Denna avhandling presenterar syntes, egenskaper och tillämpningar av två viktiga klasser av metall-organiska ramar (MOF); Lanthanid MOFs och hierarkiska porösa zeolitiska imidazolatramar (ZIFs). Materialen har karakteriseras med ett brett spektrum av tekniker inklusive diffraktion, elektronmikroskop, olika spektroskopiska tekniker, gassorption, dynamisk ljusspridning (DLS) och termogravimetrisk analys (TGA).

I kapitel 1 sammanfattas de unika egenskaperna hos MOFs och ZIFs samt deras potentiella tillämpningar. I kapitel 2 presenteras olika karakteriseringstekniker.

Kapitel 3 beskriver en familj av nya isoretiska lanthanid-MOFer syntetiseraade med hjälp av trikarboxylatligander av olika storlekar, H_3L1-H_3L4 , betecknad SUMOF-7I-IV (Ln) (SU; Stockholms universitet, Ln = La, Ce, Pr, Nd, Sm, Eu och Gd, papper I). SUMOF-7I-III (Ln) innehåller permanenta porer och uppvisar exceptionellt hög termisk och kemisk stabilitet. Luminiscensegenskaperna hos SUMOF-7IIs rapporteras (Papper II). Effekterna av Ln-joner och trikarboxylatligander samt lösningsmedel på luminescensegenskaperna undersöks. Dessutom demonstreras potentialen hos SUMOF-7II (La) för selektiv avkänning av Fe (III) joner och aminosyran tryptofan (Papper III).

Kapitel 4 presenterar ett enkelt, snabbt och skalbart tillvägagångssätt för syntesen av hierarkiska porösa zeolitiska imidazolatramar ZIF-8 och ZIF-67 med användning av trietylamin (TEA)-assisterad metod (Paper IV). Organiska färgämnen och proteiner inkapslas direkt i ZIFs med en one-pot-metod. De fotofysiska egenskaperna hos färgämnen förbättras genom inkapslingen i ZIF-8 nanopartiklar (Papper IV). ZIF-materialens porositet och ytarea kan ställas in med hjälp av olika mängder färgämne eller TEA. För att ytterligare förenkla syntesen av hierarkisk porös ZIF-8 presenteras ett mallfritt tillvägagångssätt med användning av natriumhydroxid, som vid låga koncentrationer inducerar bildningen av zinkhydroxidnitratnanoskivor som tjänar som *in situ* offermallar (Kapitel 5, Papper V). En 2D bladliknande ZIF (ZIF-L) erhålls också med hjälp av metoden. Den hierarkiska porösa ZIF-8 och ZIF-L visar god prestanda för CO₂-sorption.

List of papers

This thesis is based on the following papers: (* corresponding authors, § co-first author)

Paper I. Q. Yao; A. Bermejo Gómez; J. Su; V. Pascanu, Y. Yun; H. Zheng; H. Chen; L. Liu; **H. N. Abdelhamid**; B. Martín-Matute*; X. Zou*, Series of Highly Stable Isoreticular Lanthanide Metal-Organic Frameworks with Expanding Pore Size and Tunable Luminescent Properties, **Chemistry of Materials**, **2015**, 27, 5332–5339.

My Contribution: I synthesized and characterized MIL-103 (La).

Paper II. **H. N. Abdelhamid***, M. Wilk-kozubek, A. M. El-Zohry, A. Bermejo-Gomez, A. Valiente, B. Martín-Matute, A.-V. Mudring*, X. Zou*, Luminescence Properties for a Family of Highly Stable Lanthanide Metal-Organic Frameworks, In manuscript.

My Contribution: I played the leading role in the project. I conceived, designed, and guided the project. I performed the synthesis and characterization of the MOFs, analyzed the data and wrote the manuscript.

Paper III. **H. N. Abdelhamid***, A. Berméjo-Gómez, B. Martín-Matute, X. Zou*, A water-stable lanthanide metal-organic framework for fluorimetric detection of ferric ions and tryptophan, **Microchimica Acta**, **2017**, 184, 3363–3371.

My Contribution: I played the leading role in the project. I conceived, designed, and guided the project. I performed the materials preparation (except the synthesis of the organic linker), analyzed the data and wrote the manuscript.

Paper IV. **H. N. Abdelhamid***, H. Zhang, A. M. El-Zohry, Z. Huang*, X. Zou*, A Fast and Scalable Approach for Synthesis of Hierarchical Porous Zeolitic Imidazolate Frameworks and One-Pot Encapsulation of Target Molecules, **Inorganic Chemistry**, **2017**, 56, 9139–9146.

My Contribution: I played the leading role in the project. I conceived, designed, and guided the project. I prepared the materials, performed all data collection (except the lifetime measurements and some TEM work), analyzed the data, and wrote the manuscript.

Paper V. **H. N. Abdelhamid***, X. Zou*, Template-Free and Room Temperature Synthesis of Hierarchical Porous Zeolitic Imidazole Frameworks Nanoparticles and their CO₂ Sorption, In manuscript.

My Contribution: I played the leading role in the project. I conceived, designed, and guided the project. I synthesized the materials, analyzed the data, and wrote the manuscript.

Paper I and Paper IV reprinted with permission from ACS.

Publication not included in the thesis

1. Y. Yang, K. Shen, J.-Z Lin, Y. Zhou, Q.-Y Liu, C. Hang, **H. N. Abdelhamid**, Z-Q. Zhang*, H. Chen*, A Zn-MOF Constructed from Electron-rich π -conjugated Ligand with Interpenetrated Graphene-like Net as Efficient Nitroaromatic Sensor, **RSC Advances**, 2016, 6, 45475-45481.
2. R. M. Ashour, **H. N. Abdelhamid**, A. F. Abdel-magied, A. A. Abdel-khalek, M. M. Ali, M. Muhammed, X. Zou*, J. Dutta*, Facile and highly efficient adsorption of La(III), Nd(III), Gd(III) and Y(III) by graphene oxide: Adsorption and desorption kinetic study, **Solvent Extraction and Ion Exchange**, 2017, 1-13.
3. X. Zou*, Q. Yao, A. Bermejo Gómez, J. Su, V. Pascanu, Y. Yun; H Zheng; H. Chen; L. Liu; **H. N. Abdelhamid**; B. Martín-Matute, A series of highly stable isoreticular lanthanide metal-organic frameworks with tunable luminescence properties solved by rotation electron diffraction and X-ray diffraction, **Acta Crystallographica Section A: Foundations and Advances**, 2016, A72, s136.
4. M. Dowaidar^{§*}, **H. N. Abdelhamid**^{§*}, M. Hällbrink, X. Zou, Ü. Langel*, Graphene oxide and cell penetrating peptides for Oligonucleotides Delivery, **Biochimica et Biophysica Acta (BBA)-general subjects**, 2017, 1861 (9) 2334-2341 ([§] Co-first author)
5. M. Dowaidar^{§*}, **H. N. Abdelhamid**[§], M. Hällbrink, X. Zou*, Ü. Langel*, Magnetic nanoparticles assist self-assembly of cell penetrating peptides for oligonucleotides delivery, **Scientific Reports**, 2017, 7, 9159 ([§] Co-first author)
6. K. Hussein[§], **H. N. Abdelhamid**^{§*}, X. Zou*, Seok-Ho Hong*, Multifunctional biomedical applications of graphene oxide, Submitted, ([§] Co-first author)
7. A. Etman[§], **H.N. Abdelhamid**[§], X. Zou, J. Sun*, Facile Water Based Strategy for Synthesizing MoO_{3-x} Nanosheets: Efficient Visible Light Photocatalyst for Dye Degradation, In manuscript, ([§] Co-first author)
8. M. Naeem Iqbal, A. F. Abdel-Magied, **H. N. Abdelhamid**, A. Shatskiy, X. Zou, B. Åkermark, M. D. Kärkäs, and E. V. Johnston*, Mesoporous Ruthenium Oxide: A Heterogeneous Catalyst for Water Oxidation, Submitted
9. **H. N. Abdelhamid***, H. Zheng, X. Zou*, Surfactant assisted synthesis of MOF nanosheets, In manuscript

Contents

| | |
|---|-----------|
| Abstract | i |
| Abstrakt | ii |
| List of papers | iii |
| Contents | vi |
| Abbreviations..... | viii |
| 1. Introduction | 9 |
| 1.1. Porous solids | 9 |
| 1.2. Metal-organic frameworks (MOFs)..... | 9 |
| 1.3. Chemistry of MOFs..... | 11 |
| 1.4. Synthesis of MOFs..... | 11 |
| 1.5. What are MOFs good for? | 12 |
| 1.6. Stability of MOFs | 12 |
| 1.7. Porosity and hierarchical porous MOFs | 13 |
| 1.8. Lanthanide-based MOFs..... | 13 |
| 1.8.1. Luminescence of lanthanide MOFs | 13 |
| 1.9. Sensing and biosensing using MOFs..... | 14 |
| 1.10. Zeolitic imidazolate frameworks (ZIFs) | 14 |
| 1.10.1. Synthesis of ZIF-8..... | 15 |
| 1.10.2. Applications of ZIF-8 | 15 |
| 1.11. Carbon dioxide adsorption using MOFs..... | 15 |
| 1.12. Future trends of MOFs | 15 |
| 1.13. Aim of the work..... | 16 |
| 2. Characterization techniques for MOFs | 17 |
| 2.1. X-ray diffraction | 17 |
| 2.2. X-ray absorption spectroscopy (XAS) | 18 |
| 2.3. Electron microscopy..... | 20 |
| 2.3.1. Transmission electron microscope (TEM)..... | 20 |
| 2.3.2. Scanning electron microscope (SEM) | 21 |
| 2.4. Electron crystallography | 21 |
| 2.5. Fourier transform infrared (FT-IR) spectroscopy | 22 |
| 2.6. Nitrogen adsorption | 22 |
| 2.7. Optical spectroscopy: UV-vis and fluorescence spectroscopy | 24 |
| 2.8. Ultrafast laser spectroscopy..... | 25 |
| 2.9. Dynamic light scattering (DLS) | 25 |
| 2.10. Thermogravimetric analysis (TGA)..... | 26 |

| | |
|---|----|
| 3. Synthesis of highly stable isoreticular lanthanide MOFs (SUMOF-7) with tunable luminescence properties and their sensing applications (Paper I-III)..... | 28 |
| 3.1 Introduction..... | 28 |
| 3.2. Synthesis of highly stable isoreticular lanthanide MOFs (SUMOF-7, Paper I) | 29 |
| 3.3. Characterization of SUMOF-7II..... | 31 |
| 3.4. Luminescence properties of SUMOF-7II (Paper II)..... | 32 |
| 3.5. Emission lifetime measurements using ultrafast spectroscopy | 35 |
| 3.6. Effect of the desolvation on the emission of SUMOF-7II (La and Eu) .. | 36 |
| 3.7. Photostability | 38 |
| 3.8. Potential applications for SUMOF-7II | 38 |
| 3.9. Preparation of SUMOF-7II nanoparticles (Paper III)..... | 39 |
| 3.10. Stability of SUMOF-II (La)..... | 39 |
| 3.11. Sensing of ferric ions using SUMOF-7II (La) | 39 |
| 3.12. Characterization of interactions between SUMOF-7II and Fe (III)..... | 41 |
| 3.13. Biosensing of tryptophan..... | 43 |
| 4. One-pot encapsulation of dye/protein and synthesis of hierarchical porous ZIF-8 nanoparticles (Paper IV)..... | 44 |
| 4.1. Introduction | 44 |
| 4.2. Synthesis of ZIF-8 | 44 |
| 4.3. Characterization of ZIF-8..... | 45 |
| 4.4. Photophysical properties of dye@ZIF-8 | 49 |
| 4.5. Photostability of the dye and dye@ZIF-8 | 50 |
| 4.6. Encapsulation of a protein into ZIF-8 and the synthesis of dye@ZIF-67 | 51 |
| 5. Template-free and room temperature synthesis of hierarchical porous zeolithic imidazole framework nanoparticles and their CO ₂ sorption (Paper V) | 53 |
| 5.1. Introduction | 53 |
| 5.2. Synthesis of hierarchical porous ZIF-8 using template-free approach .. | 53 |
| 5.3. Observation of intermediate phases..... | 53 |
| 5.4. Application of ZIF-8 and ZIF-L for CO ₂ sorption..... | 60 |
| 6. Conclusions | 61 |
| 7. Future perspectives..... | 62 |
| 8. Acknowledgements | 63 |
| 9. References | 65 |

Abbreviations

| | |
|--------|---|
| ACS | American Chemical Society |
| BASF | Baden Aniline and Soda Factory |
| BET | Brunauer–Emmett–Teller |
| CVD | Chemical vapor deposition |
| COFs | Covalent organic frameworks |
| CSD | Cambridge Structural Database |
| DMF | <i>N, N</i> -Dimethylformamide |
| ED | Electron diffraction |
| EXAFS | Extended X-ray absorption fine structure |
| IUPAC | International Union of Pure and Applied Chemistry |
| MeOH | Methanol |
| MIL | Matérial Institut Lavoisier |
| MOFs | Metal–organic frameworks |
| MRI | Magnetic resonance imaging |
| NEXAFS | Near-edge X-ray absorption fine structure |
| NMR | Nuclear magnetic resonance |
| NLDFT | Non-local Density Function Theory |
| PSE | Postsynthetic exchange |
| PSM | Postsynthetic modification |
| PSMet | Postsynthetic metallation |
| SBU | Secondary building unit |
| SEM | Scanning electron microscopy |
| STY | Space time yields |
| TEM | Transmission electron microscopy |
| TGA | Thermogravimetric analysis |
| UiO | University of Oslo |
| XAS | X-ray absorption spectroscopy |
| PXRD | Powder X-ray diffraction |
| ZIF | Zeolithic imidazolate framework |

1. Introduction

1.1. Porous solids

Porous materials are solid with pore structures¹. The porous materials can be classified based on the pore size to micropore (< 2 nm), mesopore (2 and 50 nm), and macropore (> 50 nm)¹.

Porous materials contributed in the advancements of several applications including catalysis, separations, energy-related technologies, and biomedicine. There are several types of porous materials including zeolites, silica, carbons, and metal-organic frameworks (MOFs)². Description of these classes is summarized in Figure 1.1.

| | Zeolites | Metal-organic frameworks ² | Covalent-organic frameworks | Porous organic polymers | Porous molecular solids |
|------------------------------|--|---|--|---|--|
| Porosity | Microporous or mesoporous ² ; narrow pore size distributions | Can be ultraporous/ ² /mesoporous; narrow pore size distributions | Can be ultraporous/ ² /mesoporous; narrow pore size distributions | Can be ultraporous/ ² /mostly microporous; broader pore sizes | Can be ultraporous/ ² /mesoporous, but this is rare so far |
| Crystallinity | Typically high; can also be amorphous | Typically high | Modest to high | Amorphous | High, but amorphous examples, too |
| Stability | Thermal stability generally excellent; can be acid/base sensitive | Poor to good; growing number of water-stable MOFs | Boronates ² generally poor; imines ² generally good | Good to excellent, especially hydrothermal | Generally poor, though isolated examples of hydrothermal stability |
| Modularity/ diversity | High; new structures can be based on known zeotypes ² | Very high even for single-linker MOFs; also multivariate MOFs ²⁰ | In principle high; less developed than MOFs | Very high; multiple linkers and linker functions possible ²⁰ | Cocrystals possible ²⁰ ; not widely exemplified yet |
| Processing | Insoluble, but technologies for films, composites and pellets are well developed | Insoluble, though many recent examples of composite and films | Insoluble, but examples of surface growth | Modest processability, with exception of soluble PIMs ²¹ | Soluble, as for PIMs could be advantage or disadvantage, depending on function |
| Designability | Excellent, though design of organic templates can still be challenging ²² | Excellent; isoreticular principles of node/strut metal-organic bonding are well developed ²² | In principle good, as for MOFs; isoreticular approach possible | Composition control good; 3-D structure control more challenging | Isolated cage can encode functions, ²³ but no general isoreticular strategy |
| Unique selling points | Stability; low cost, commercially proven technology | Structural and chemical control for diverse range of materials | Electronic properties | Extended conjugation for CMPs ²⁴ ; solution-processing for PIMs | Solution processing; physical properties intrinsic to cages |
| Summary | Developed but still actively growing area; zeolites have major commercial importance | Established and highly active field; as yet, no large-scale applications | Much less developed than MOFs, but early promise for organic electronics | Rapidly growing in number; diverse chemistry, commercial application for PIMs ²⁵ | New area with fewer examples, but early promise for specific molecular separations |

Figure 1.1. Classes of porous materials. Image was reprinted with permission from Ref.². Copyright belongs to AAAS.

1.2. Metal-organic frameworks (MOFs)

MOFs are hybrid porous materials that consist of inorganic and organic moieties^{2,3}. They are formed via coordination of metal cations

(primary building unit, PBU) or metal clusters (secondary building unit, SBU) and organic linkers having more than one binding site⁴. MOFs are unique porous materials and combine the advantages of inorganic (zeolites) and organic based porous materials (covalent organic frameworks (COFs), porous organic polymers or porous molecular solids, Figure 1.1). MOFs with a permanent porosity attracted the community of porous materials⁵. They offer unique chemical and physical properties. MOFs provide ultrahigh porosity, tunable structure, and in many cases good thermal or chemical stability (Figure 1.2)⁶. MOFs cover a vast number of different disciplines including chemistry, materials science, chemical engineering, and others. The synthesis, structural description, surface modification, and applications of MOFs are reviewed extensively⁷⁻¹⁵. A database "MOFomics" is developed to characterize the pore structures of MOFs¹⁶. A study based on Cambridge Structural Database (CSD) identified and extracted information on ca. 70 000 MOFs¹⁷.

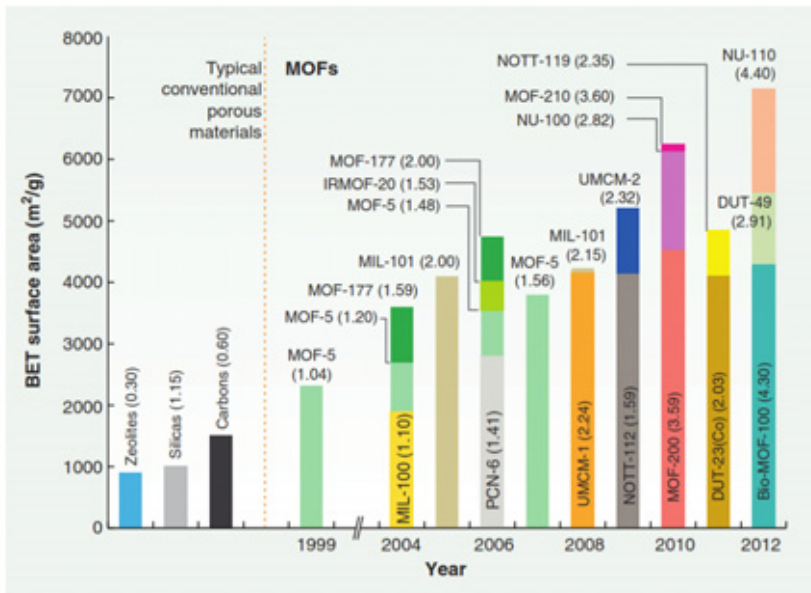


Figure 1.2. Evolution of MOFs with ultrahigh BET surface areas compared to conventional porous materials. The values in parentheses stand for the pore volume (cm^3/g). Figure reprinted with permission from Ref.¹⁸. Copyright belongs to AAAS.

1.3. Chemistry of MOFs

The understanding of the coordination chemistry was initiated by Alfred Werner who received the Nobel Prize in Chemistry 1913¹⁹. Based on the assumption of the presence of two valences; primary (oxidation state) and secondary valence (coordination number), an element tends to satisfy both valences. Hofmann clathrates were considered as the first coordination networks ($[\text{Ni}(\text{CN})_2(\text{NH}_3)] \cdot \text{C}_6\text{H}_6$)^{20,21}.

In general, a metal satisfies its two valences via coordination to organic moieties with coordinating groups such as carboxylic, cyano, hydroxyl, amine, or carbonyl groups²². The metal-linker bond defines the MOF chemistry. Strong metal-linker bond offers permanent porosity, and promotes high framework stability under conditions such as acidic/basic media, elevated temperature, or light radiations.

1.4. Synthesis of MOFs

Industry concerns mainly the materials functionality and operational costs rather than the materials classification. The synthesis procedure of MOFs determines the materials cost. MOF synthesis is often a trial-and-error process. There are several methods for the synthesis of MOFs which can be subdivided into traditional methods including thermal methods (e.g., solvothermal, hydrothermal, ionothermal), mechanical procedure (e.g., milling), or new methods including microwave, chemical vapor deposition (CVD), and ultrasonic. Traditional methods, such as thermal-based method, electrochemical, or mechanochemical, produce high-quality materials. On the other hand, methods such as microwave or ultrasonic offer fast heating of the solutions and high space time yields (STY). However, the material qualities are low compared to traditional methods. The standard method for the synthesis of MOFs is the solvothermal method. MOFs can be modified using post synthetic methods (PSM) including cation exchange²³, and post-synthetic metalation (PSMet)²⁴.

The low solubility of organic linkers requires the use of an organic solvent that sometimes blocks the pores. The presence of impurities or unreacted metals or linkers inside the pore is usually a frequent problem. Thus, there are several methods to remove residual solvents or unreacted reagents inside the pores including solvent exchange. This process sometimes is tedious and leads to the collapse of the frameworks.

Many reaction conditions influence the synthetic procedure and the properties of the final MOF products^{25,26}. The reaction conditions can be modified to improve the material crystallinity; decrease the reaction temperature or time, and slow down or enhance linker deprotonation rate. There are many methods for modulating the materials properties including size, morphology, porosity, and surface area. The modulation can be achieved using different methods including a combination of different solvents²⁷, template molecule²⁸, pH adjustment²⁹, and the coordination equilibria between framework components³⁰.

Large scale synthesis of MOFs faces limitations such as low synthetic rates (STY typically < 300 kg·m⁻³·d⁻¹). The current synthesis approaches require in most cases harsh processing conditions (presence of acids (HF, HCl ...), etc.), or high temperature and pressure)³¹. New environmentally friendly methods with high STY are highly desirable.

1.5. What are MOFs good for?

It is hard to find a porous material that fits the requirements of all applications². MOFs advanced many fields including biochemical applications³², devices fabrication³³, gas storage³⁴, photocatalysis³⁵, luminescence sensing and light emitting³⁶, lithium ion batteries and supercapacitors³⁷.

1.6. Stability of MOFs

Thermal and chemical stability of the MOFs is often required for applications in industry. The stability of MOFs depends on many parameters including the bond strength of metal-linker interactions, coordination number, the presence of impurities, framework dimensionality, and framework interpenetration³⁸. The bond strength of metal-linker interactions for the same linker depends on the metal properties regarding the type of the coordinating orbitals (s, p, d, or f), and oxidation state (I, II, IV...etc.). Metals of d orbitals (transitions elements) and f orbitals (lanthanides and actinides) often form stable MOFs. MOFs with high oxidation state metals such as Zr (IV) (UiO-66) show high thermal and chemical stability.

The coordination affinity of certain molecules such as water decreases the stability of some MOFs. Several approaches, including 1) selecting metals that tend to have high coordination number, 2) increasing the hydrophobicity of MOFs using hydrophobic organic link-

ers and 3) coating the material surface with a hydrophobic polymer, were developed to improve the water stability of MOFs³⁹.

1.7. Porosity and hierarchical porous MOFs

Several synthetic procedures were developed for the synthesis of MOFs with mesoporosity or interconnected micro/mesoporosity (hierarchical porous MOFs)⁴⁰. The conventional synthesis methods for mesoporous MOFs are ligand-extension method (Figure 1.3)⁴¹⁻⁴⁴, CO₂ expanded liquid⁴⁵, use of organic molecules as template⁴⁶, and competitive ligand strategy⁴⁷. These methods required the design of lengthy organic linkers^{41,42,48}, or the use of template molecules⁴⁶.

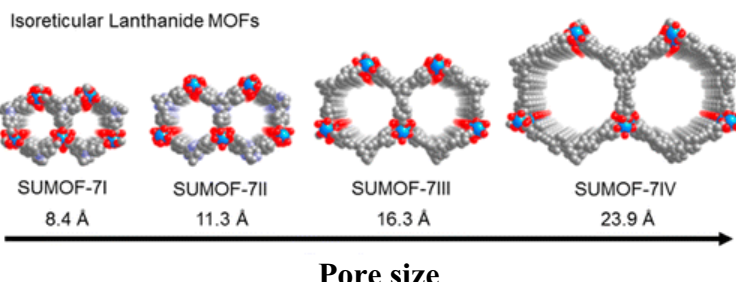


Figure 1.3 Linker-extension method for the synthesis of isoreticular lanthanide MOFs (SUMOF-7, paper I). Figure reprinted with permission from Ref.⁴².

1.8. Lanthanide-based MOFs

Lanthanide-based MOFs possess several advantages and promote the advances of many applications. For more details of lanthanide MOFs including their syntheses, properties, and potential applications, the reader is recommended to read the book cited in Ref.⁴⁹.

1.8.1. Luminescence of lanthanide MOFs

Luminescence properties of MOFs were used in several applications including sensing, biosensing, and light harvesting^{50,51}. Lanthanide MOFs offer several advantages. First, there are many MOFs with suitable chromophore sensitizers and metal centers that fit several applications. Second, lanthanide MOFs show remarkable photophysical properties such as high quantum yield. Third, lanthanide MOFs have tunable energy and cover the entire spectrum (UV-visible-near infra-

red ranges)⁵². Fourth, increasing the linker's rigidity via coordination with metal centers offers high energy transfer⁵³. For more details on the photophysical properties of MOFs, the reader is advised to refer to the reviews in the cited references^{36,54–56}. In general, electron transitions of lanthanide based MOFs can be divided into four types⁵⁷:

1. Broad intramolecular luminescence emission of the organic linker.
2. Sharp intraconfigurational 4f–4f electron transitions featuring rearrangement of the electrons within the 4fⁿ subshell.
3. Broader 4f–5d transitions when a 4f electron is moved into an empty 5d orbital.
4. Broad charge transfer (CT) transitions, during which one electron is transferred from the metal ion to the bonded ligands (metal-to-ligand charge transfer [MLCT]) or vice versa (ligand to-metal charge transfer [LMCT]).

Lanthanide-based MOFs offer sensitive signal change upon the interaction with target species. MOFs provide diverse and easily modifiable structures and topology, permanent porosity, and tunable electronic band gaps. Lanthanide MOFs possess long lifetime emissions, large Stokes shifts, and sharp line emissions.

1.9. Sensing and biosensing using MOFs

Applications of MOFs for sensing and biosensing are promising⁵⁸. MOFs were applied for sensing of explosive species^{51,59}, gases⁶⁰, chemical vapors⁶¹, and metal ions^{62,63}. MOFs offer sensitive and selective detection of several target species. They provide multi-functionalities, are easy for device fabrication and can be applied in several analytical techniques including fluorescence, UV-vis absorption, mass spectrometry and others⁶⁴.

1.10. Zeolitic imidazolate frameworks (ZIFs)

ZIFs are a subclass of MOFs⁶⁵. The M–IM–M angle (where IM is an imidazole based linker (e.g. 2-methylimidazole (Hmim)), and M is the metal center) is similar to the Si–O–Si angle (145°) found in zeolites⁶⁵. Synthesis and applications of ZIFs were reviewed in Ref.⁶⁶.

ZIFs have permanent porosity and high thermal (> 550 °C under N₂) and chemical stability. ZIF-8 has both basic (4.99 μmol·g⁻¹, CO₂-temperature program desorption (TPD)) and acidic characters (0.405

$\mu\text{mol}\cdot\text{g}^{-1}$, NH₃-TPD)⁶⁷. ZIF-8 material has large surface area ($> 1531 \text{ cm}^2\cdot\text{g}^{-1}$), and pore volume $0.485 \text{ cm}^3\cdot\text{g}^{-1}$ with the largest pore and pore opening diameter of 11.4 and 3.4 Å, respectively⁶⁵.

1.10.1. Synthesis of ZIF-8

BASF commercialized microporous ZIF-8. Sigma Aldrich trades the material under the trademark Basolite® (Basolite-Z1200). ZIF-8 has been synthesized using several methods including CVD⁶⁸, solvothermal method⁶⁵, T-type micromixer⁶⁹, microwave⁷⁰, steam-assisted conversion⁷¹, mechanochemical approach⁷², and sonochemical method⁷³. ZIF-8 was synthesized in organic solvents (dimethyl formamide, DMF)⁶⁵ and water⁷⁴. Water not only is a green solvent, but also does not block the small pore of ZIF-8 as do organic solvents.

1.10.2. Applications of ZIF-8

ZIF-8 was used for catalysis including transesterification of vegetable oil⁷⁵, Knoevenagel reaction⁷⁶, and dehydrogenation⁷⁷, as well as for adsorption of gases⁷⁸, small alcohol^{79,80}, pollutants⁸¹, and metals⁸². It has also been applied for sensing⁶¹, drug delivery⁸³, devices fabrication⁸⁴, and photovoltaic cells⁸⁵.

1.11. Carbon dioxide adsorption using MOFs

Carbon dioxide mitigation or separation is an important process for environmental concerns and industrial applications^{86,87}. There are several approaches including adsorption-based approaches to capture CO₂.

Sorption of CO₂ using MOFs is promising for reducing anthropogenic CO₂ emission and lowering the concentration of greenhouse gases in the atmosphere⁸⁶⁻⁸⁹. Compared to other porous materials, MOFs have demonstrated impressive results for CO₂ uptakes with high selectivity⁸⁶⁻⁹⁰.

1.12. Future trends of MOFs

The applications of MOFs will be impressive by all predictions. Most of the latest trends will focus on the investigation, understanding, and improvement of MOFs properties. Several industrial applications are

undergoing. This progress cannot be achieved without large-scale production.

Large scale production of MOFs faces several challenges. The first challenge is the availability of inexpensive organic linkers. Cheap and commercial organic linkers are highly required. Most of the reported linkers are very sophisticated, which are not available on the industrial scale. The synthesis often needs organic solvents. Water or solvent-free methods should be investigated. The second challenge is the synthesis procedure. New technologies should be implemented to achieve large scale production⁹¹. An important key for industrial applications is the material cost. The prices for those commercialized MOFs are from 1 to 35 US \$·g⁻¹⁸⁹. A suitable selection of raw materials and the synthesis method may reduce the material cost.

1.13. Aim of the work

The first part of this thesis explores the synthesis, properties and applications of stable MOFs using lanthanides as the metal clusters. The choice of lanthanide elements for new linker series (H₃L1-H₃L4) offers stable frameworks⁹². The extension of the organic linker offers an increase of the material porosity (8.4-23.9 Å). The lanthanide MOFs show promising photophysical properties and provide applications such as sensing and biosensing of metal ions and amino acids, respectively.

The second part of this thesis develops simple synthesis approaches for the synthesis of hierarchical porous ZIF-8 using template-based and template-free methods. The template-based method provides simple one-pot encapsulation of organic dyes or proteins. The encapsulation of organic dye improves their photophysical properties. The method is also applied for the synthesis of dye@ZIF-67 (Co-based ZIF). In order to avoid the use of template molecules such as organic dye or protein, a template-free approach is developed using NaOH that induce the formation of *in situ* sacrificial template. The template-free method is simple, requires only controlled concentration of NaOH, and avoids extra steps of the template removal. The method can be applied to synthesize 2D leaf-like ZIF (ZIF-L). The template-based and template-free methods offer tunable hierarchical porous ZIF-8. Application of hierarchical porous ZIF-8 or ZIF-L for CO₂ sorption was also reported.

2. Characterization techniques for MOFs

This chapter introduces various techniques that were used for the characterization of MOFs. A brief introduction of each technique will be discussed, and links to books or review articles will also be mentioned for further information.

2.1. X-ray diffraction

X-ray beams (with a wavelength of 0.01-10 nm) are widely used for the materials characterization. The X-ray beams be diffracted, or absorbed after the interaction with matter. The interactions depend on the energy of the beam and the nature of the matter.

Diffraction using X-ray is a known technique for the characterization of crystalline materials including MOFs. Single crystal X-ray diffraction (SCXRD) and powder X-ray diffraction (PXRD) are widely used to solve the structure of crystalline MOFs. SCXRD requires single crystal with the size of 5-250 μm . It is a difficult task to produce large crystals of MOFs with high quality and good stability for SCXRD⁹³. On the other hand, PXRD requires a specimen containing an infinite number of individual small crystals with an infinite number of orientations.

PXRD is also used as a routine technique for the confirmation of the phase purity of known MOFs. It can be used to name the material phase after applications such as catalysis, or sensing. For instance, interactions of FeCl_3 or $\text{Fe}(\text{acetate})_3$ with SUMOF-7II (La) show no change in the crystallinity (Figure 2.1).

PXRD was used to optimize the synthesis condition of ZIF-8 (Figure 2.2). PXRD patterns demonstrate that the optimum Hmim: Zn molar ratio for the formation of ZIF-8 in the presence of triethylamine (TEA) is 2-50 (Figure 2.2).

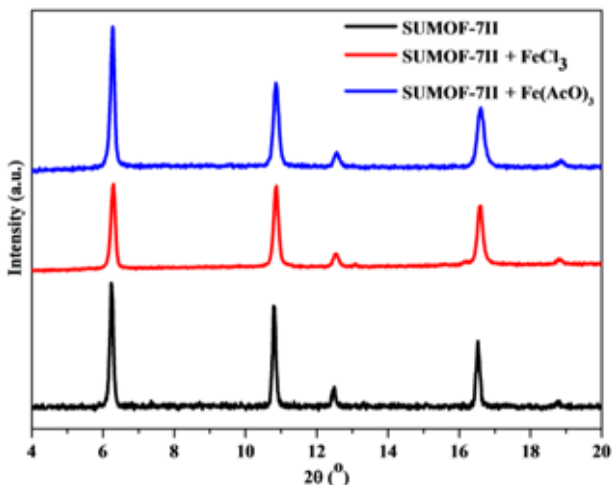


Figure 2.1. PXRD patterns of SUMOF-7II (La) and its interactions with a solution of FeCl_3 or $\text{Fe}(\text{acetate})_3$. Figure reprinted with permission from Ref.⁹⁴ (Paper III).

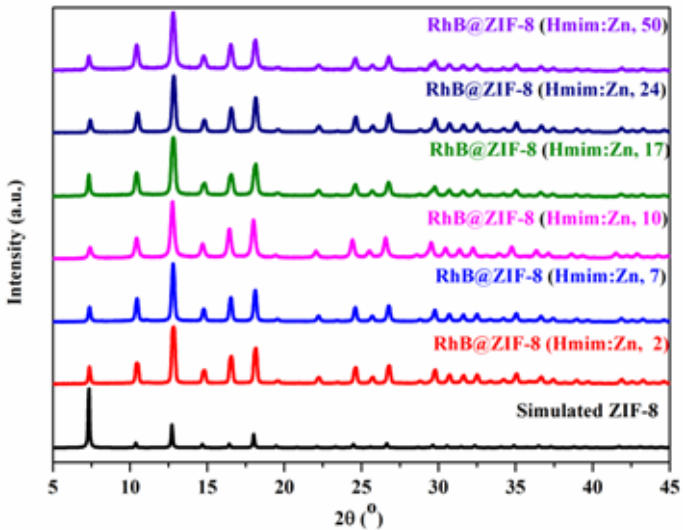


Figure 2.2. PXRD patterns of ZIF-8 synthesized using different Hmim: Zn molar ratios in the presence of rhodamine B (RhB) dye. Figure reprinted with permission from Ref.⁹⁵ (Paper IV).

2.2. X-ray absorption spectroscopy (XAS)

XAS is a synchrotron based X-ray technique. XAS is a useful method for determination of the local geometric and electronic structure of an element in a matter^{96,97}. It is applicable for solids, gases and liquids. It

is suitable for both amorphous and crystalline materials. The principle of XAS is based on the excitation of the core electron (the principal quantum numbers $n = 1, 2$, and 3 , corresponding to the K-, L-, and M-edges) of the target atom using the energy of 0.1-100 keV photon energy. The electron of the investigated atom is excited to the empty orbital, resulting in a "pre-edge" peak. The excited electron interacts with neighboring atoms and forms constructive and destructive interferences (Figure 2.3).

For more details of XAS principles and applications, it is recommended to read the book written by G. Bunker⁹⁶ or the Ph.D. thesis of F. Jalilehvand⁹⁷. A typical XAS spectrum shows three main regions defined as;

- 1) The pre-edge region; It is due to the excitation of the inner electron to the lowest unoccupied states.
- 2) X-ray absorption near-edge structure (XANES) region; It is a sharp peak that stands for the core shell electron transitions to quasi-bound states.
- 3) Extended X-ray absorption fine structure (EXAFS) region; It refers to the scattering of the ejected electron by neighboring atoms.

X-ray absorption spectra of FeCl_3 and $\text{FeCl}_3@\text{SUMOF-7II}$ (La) were reported for the K-edge (E equal to 7112 eV) of Fe^{3+} (Figure 2.3). The pre-edge is attributed to the $1s-3d$ transition. The peaks of Fourier transform refer to $\text{Fe}-\text{Cl}$ and $\text{Fe}-\text{O}$ corresponding to an average bond distance of 2.30 \AA and 1.70 \AA , respectively (Figure 2.3). EXAFS data demonstrate no change of Fe^{3+} oxidation state and confirm that there is no cation exchange with La^{3+} clusters of SUMOF-7II.

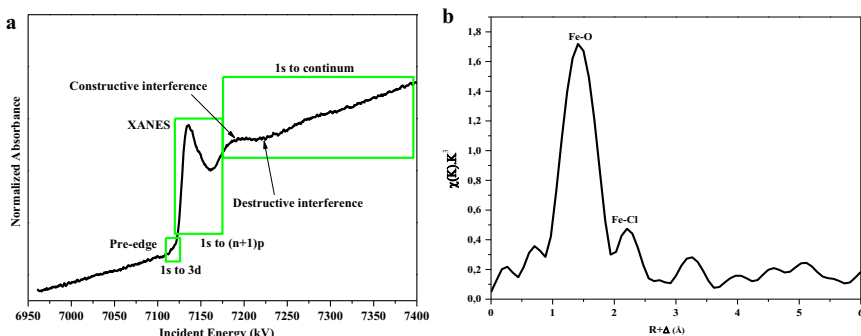


Figure 2.3. a) Typical XAS spectrum of $\text{FeCl}_3@\text{SUMOF-7II}$ and b) Fourier transform EXAFS spectrum of $\text{FeCl}_3@\text{SUMOF-7II}$. Figure reprinted from Ref.⁹⁴ (Paper III).

2.3. Electron microscopy

Electron microscopy (EM), including transmission electron microscopy (TEM), and scanning electron microscopy (SEM), are useful techniques for the investigation of particle size, morphology, crystal structure, and pore size distribution. An electron microscope uses a beam of accelerated electrons as a source of illumination. Because of the dual function of the electron; particle and wave, electron beams can be controlled using electrostatic and electromagnetic lenses. Electrons have a very short wavelength (0.037-0.020 Å, depending on the accelerating voltage, typically ~100–300 kV). Thus, EM offers high resolving power for small particles.

2.3.1. Transmission electron microscope (TEM)

A TEM can reach a resolution of 50 pm and magnification up to 10,000,000x⁹⁸. The fundamentals and the construction of TEM can be found in the book cited in Ref.⁹⁹. TEM requires a sample with high stability (for electron beam and in vacuum) and thin thickness (<100 nm).

TEM images of ZIF-8 synthesized using different concentrations of RhB dye show the material morphology and particle sizes (Figure 2.4). TEM images confirm the presence of mesopores and demonstrate their distribution within the crystals (Figure 2.4). The mesopore density increases with the increase of the dye concentrations. They show the particle sizes of 50-200 nm.

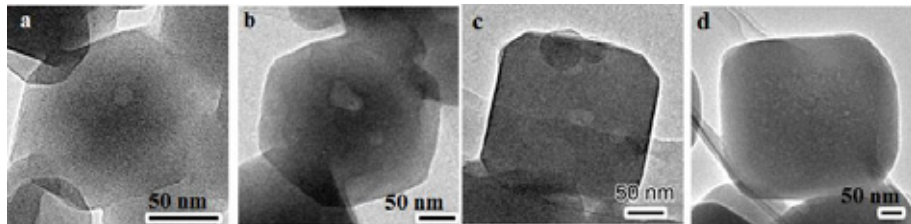


Figure 2.4. TEM images of RhB@ZIF-8 synthesized using different RhB amounts (a) 2 μmol, (b) 8 μmol, (c) 20 μmol, and (d) 30 μmol. The molar ratio of Hmim: Zn: TEA is 10:1:1. Figure reprinted with permission from Ref.⁹⁵ (Paper IV).

2.3.2. Scanning electron microscope (SEM)

SEM images are produced via probing the specimen surface using a focused electron beam. The specimen should be conductive; therefore, non-conductive materials require a conductive coating. SEM allows imaging of larger area compared to TEM. The morphology of the examined materials is highly resolved in SEM image compared to TEM.

SEM image shows that the morphology of SUMOF-7II (La) is rod-like with a trigonal end (Figure 2.5). After grinding and sonication of SUMOF-7II (La) crystals in ethanol, the SUMOF-7II (La) turned to nanoparticles with particle sizes of ~60 nm (Figure 2.5).

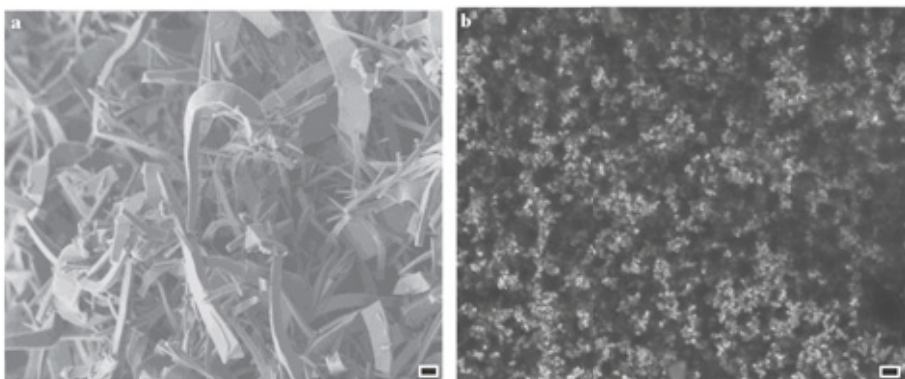


Figure 2.5. SEM images of SUMOF-7II (La) a) as synthesized and b) after grinding and ultrasonic dispersion in ethanol. The scale bars are 1 μm . Figure reprinted from Ref.⁹⁴ (Paper III).

2.4. Electron crystallography

Electron diffraction (ED) is a paramount important technique for characterization of a tiny crystalline material. ED can be used to figure out the arrangement of atoms in solids using an electron beam. More details about electron crystallography can be found in the book cited in Ref.¹⁰⁰. The research area of ED is growing rapidly, and more advanced techniques have been introduced¹⁰⁰. Electron diffraction was used to solve the structure of new isoreticular MOFs (SUMOF-7, paper I)⁴².

2.5. Fourier transform infrared (FT-IR) spectroscopy

FT-IR spectroscopy is a routine technique for the characterization of MOFs. Infrared spectroscopy can be used to confirm the coordination of the metal centers and the linker. It gives information about the available functional groups of MOFs. FT-IR spectra offer useful information about the presence of impurities or unreacted linkers. It can be used for the characterization of noncrystalline or amorphous samples.

FT-IR spectra of the isostructural SUMOF-7II (Ln) ($\text{Ln} = \text{La, Ce, Pr, Nd, Sm, Eu, Gd}$) and RhB encapsulated ZIF-8 are shown in Figure 2.6. The peaks of $\text{Ln}-\text{O}$ and $\text{Zn}-\text{N}$ at wavenumbers of 480 and 420 cm^{-1} , respectively confirm the coordination of the metal (lanthanide or zinc) and the organic linker ($\text{H}_3\text{L}2$ or Hmim, respectively). The peaks at ~ 1554 and 1364 cm^{-1} are assigned as asymmetric ($\nu_a(\text{COO})$) and symmetric ($\nu_s(\text{COO})$) stretching, respectively. The absence of peaks at 1227 cm^{-1} (referring to $\text{C}-\text{O}-\text{H}$) confirms that the materials do not have unreacted organic linkers.

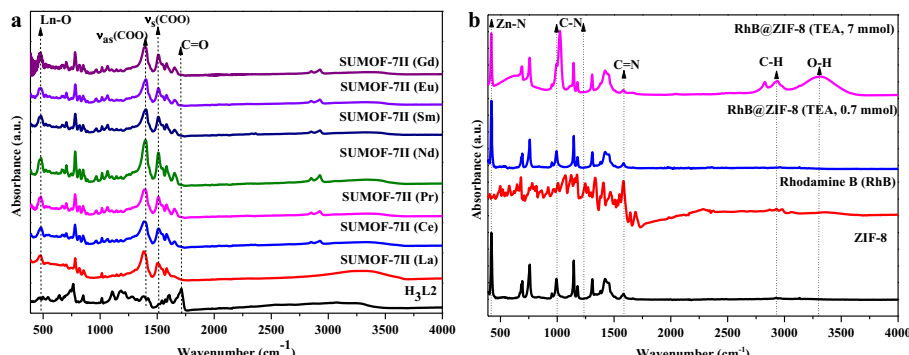


Figure 2.6. FT-IR spectra of a) SUMOF-7II (Paper II) and b) RhB@ZIF-8. Figure (b) reprinted with permission from Ref.⁹⁵ (Paper IV).

2.6. Nitrogen adsorption

The adsorption process is an enrichment of a solid surface (adsorbent) by gas or liquid molecules (adsorbate). Adsorption is an interface phenomenon; however, it can take place into the interior of the solid. There are two types of adsorption; chemo-sorption (including the formation of covalent bonds) and physio-sorption (including noncovalent bonds such as electrostatic forces, hydrogen bonds, or van der Waals

forces). The adsorption process is described using an isotherm curve at a constant temperature. The isotherm is a plot of the amount of adsorbate on the adsorbent as a function of its pressure (gas) or concentration (liquid). The isotherm curve usually records the adsorption-desorption process. The isotherm can give information of the state of the material porosity (either porous (microporous, mesoporous, or macroporous), or nonporous), surface area, and pore size distribution. There are several books which discussed in details adsorption and its applications^{1,101}.

Several theories including Henry, Freundlich, Langmuir, and Brunauer-Emmett-Teller (BET) were developed to explain the adsorption isotherm¹⁰¹. Langmuir and BET assume the formation of monolayer capacity. The BET method, using nitrogen gas as adsorbate, has been considered as a standard method for calculating the specific surface area of porous solids (ISO 9277). The materials surface area depends on the material properties such as porosity, particle size, morphology, and surface roughness. The calculation of the specific surface area assumes the formation of a complete monolayer in a close-packed 'liquid' state at 77 K¹⁰².

Pore size distribution is defined according to IUPAC as "The distribution of pore volume concerning pore size; alternatively, it may be defined by the related distribution of pore area with respect to pore size"¹⁰³. Capillary condensation occurs in the pores at $p/p_0 > 0.8$. It handles the filling of mesopores and macropores. The material takes up more adsorbate than the corresponding volume of the multilayer. The capillary condensation depends on the shape of the pore (slit or cylinder). There are several empirical models for the pore size distribution¹⁰⁴. Pore size distribution can be calculated using Barrett-Joyner-Halenda (BJH), Polanyi and Dubinin (DR method), Stoeckli, Horvath-Kawazoe, and Density Functional Theory (DFT)/non-local DFT (NLDFT). Precise pore size analysis is complicated due to 1) the changes in the pore volume of the adsorbent during the measurements, 2) swelling of non-rigid pores, 3) irreversible uptake of molecules in the pores, and 4) interaction between the gas molecules and adsorbent.

MOFs posses high specific surface area compared to other porous materials (Figure 1.2)¹⁸. For instance, MOF-210 has BET and Langmuir specific surface areas of 6,240 and 10,400 m²/g, respectively¹⁰⁵. MOFs show higher pore volume compared to traditional porous materials such as zeolites, activated carbon, or silica (Figure 1.2).

N₂ adsorption-desorption isotherms characterize the hierarchical porous structure of dye@ZIF-8 (Figure 2.7). The surface area of

RhB@ZIF-8 is increased with the increase of the dye loadings (Figure 2.7), the amount of TEA (Figure 2.7), or using reflux (Figure 2.7). RhB@ZIF-8 after the reflux treatment shows a higher pore volume compared to as-synthesized RhB@ZIF-8 (Figure 2.7). DFT analysis shows broad pore size distributions (5-60 nm) with the largest volume at 40 nm after reflux or at 15 and 40 nm using high TEA concentrations (Figure 2.7). Pore size distribution confirms the creation of micropore-mesopore ZIF-8 (hierarchical porous ZIF-8).

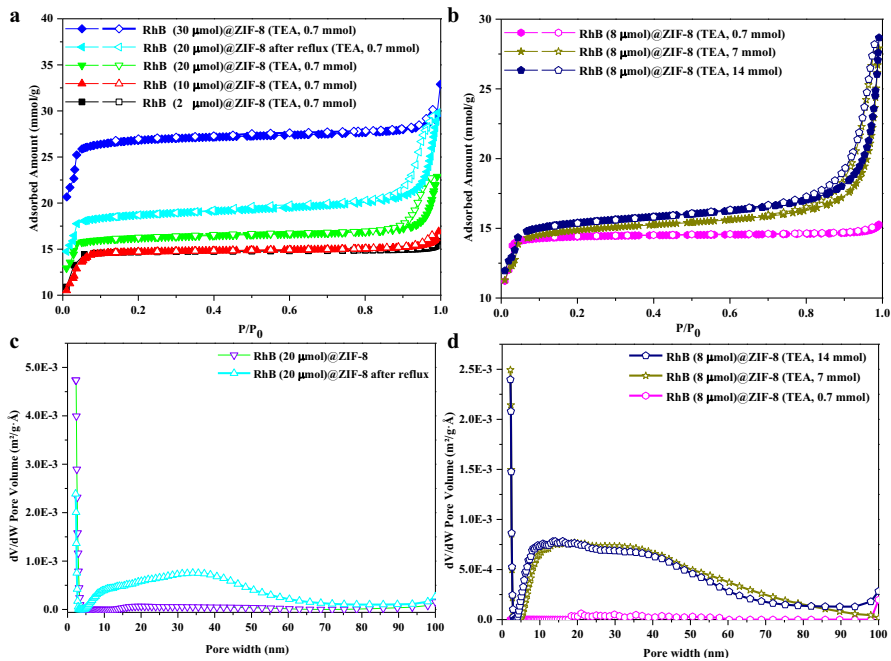


Figure 2.7. N₂ adsorption (closed symbol)-desorption (open symbol) of RhB@ZIF-8 using a) RhB and b) TEA, and c-d) Pore size distribution using DFT method. Figure reprinted with permission from Ref.⁹⁵ (Paper IV).

2.7. Optical spectroscopy: UV-vis and fluorescence spectroscopy

Optical spectroscopy including UV-vis absorption (characterizing electron transition from ground state to excited state) and fluorescence spectroscopy (characterizing electron transition from excited state to ground state) characterize the optical properties of MOFs.

UV-vis spectroscopy shows absorption maxima at 285 and 288 nm for H₃L2 and SUMOF-7II (La), respectively (Figure 2.8). SUMOF-7II

(La) shows maximum fluorescence emission (at 374 nm) at an excitation wavelength of 285 nm (Figure 2.8).

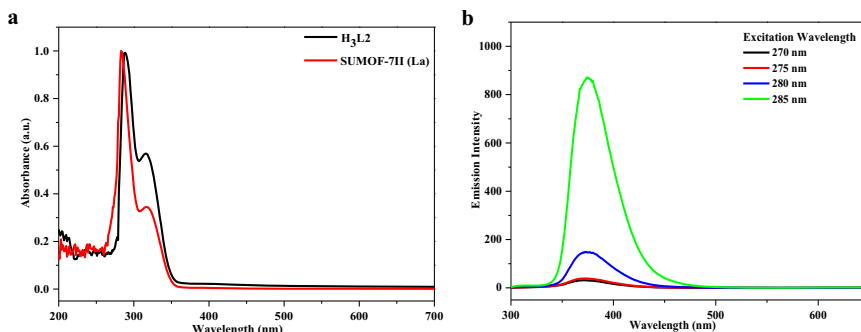


Figure 2.8. a) UV-vis absorption of $\text{H}_3\text{L}2$ and SUMOF-7II (II) and b) fluorescence emission of SUMOF-7II (La). Figure reprinted from Ref.⁹⁴ (Paper III).

2.8. Ultrafast laser spectroscopy

Ultrafast laser spectroscopy uses ultrashort laser pulses (nanosecond-attosecond) to characterize excitation lifetime, and dynamics of charge carriers, atoms, and molecules¹⁰⁶. Time-correlated single photon counting (TCSPC) analyzes the relaxation process of an excited state to a lower energy state using single photon counting. TCSPC measures the emission lifetime of isostructural MOFs (SUMOF-7II (Ln), Ln = La, Ce, Pr, Nd, Sm, Eu, Nd, and Gd) and the organic linker ($\text{H}_3\text{L}2$, Figure 2.9). The exponential decay curve shows the typical decay process of the organic linker and SUMOF-7II (La) (Figure 2.9). TCSPC records the time of the first photon from the sample molecule relative to the light pulse (instrument response function, IRF). The organic linker ($\text{H}_3\text{L}2$) shows a lifetime of 800 ps (Figure 2.9). SUMOF-7IIs of near infrared lanthanide (Pr, or Nd) show the shortest lifetime (Figure 2.9).

2.9. Dynamic light scattering (DLS)

DLS, also known as photon correlation spectroscopy (PCS), is a laser based technique used to determine the hydrodynamic particle size distribution of a suspension. DLS analysis of dispersed SUMOF-7II (La) shows that the particle size is 50-80 nm with an average size of 65 nm (Figure 2.10).

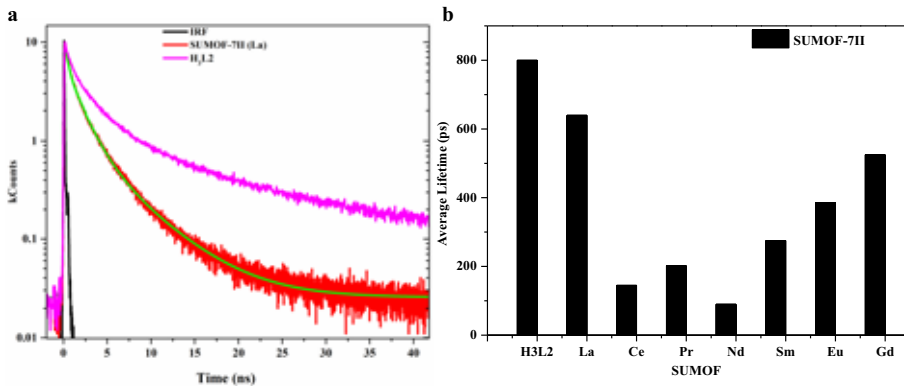


Figure 2.9. a) Typical lifetime decay for $\text{H}_3\text{L}2$ and SUMOF-7II (La), and b) the lifetimes of isostructural SUMOF-7II (La-Gd). Figure reprinted from Paper II.

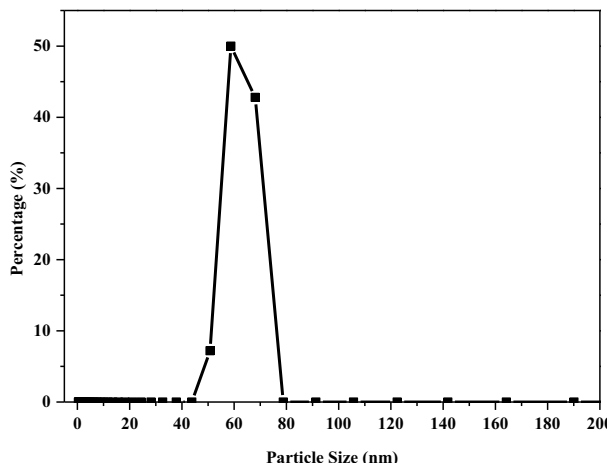


Figure 2.10. DLS analysis of ground SUMOF-7II dispersed in ethanol (95 %). Figure reprinted from Ref.⁹⁴ (Paper III).

2.10. Thermogravimetric analysis (TGA)

TGA can be used to study the thermal stability of MOFs. TGA records the weight loss of the investigated MOFs with the increase of temperature under gas flow (N_2 or air). A typical TGA curve shows the weight loss percentage vs temperature (Figure 2.11). TGA gives information of (1) the MOF crystallinity; a sharp decomposition rate indicates high crystallinity; (2) the temperature of decomposition, (3)

determination of organic and inorganic contents in a MOF, (4) the sample purity; the presence of impurities decreases the decomposition temperature, and (5) the tendency of the MOFs to oxidation at elevated temperature. An advanced technique based on TGA such as TPD offer information about acidity and basicity of MOFs.

TGA curves of isostructural SUMOF-7II series (La, Ce, Pr, Nd, Sm, Eu, Nd, and Gd) show that the materials have high thermal stability (> 450 °C, Figure 2.11(a)). Figure 2.11 indicates that the thermal stabilities of SUMOF-7II (Ln) are in the order of Nd > Pr ≈ Sm > La ≈ Ce ≈ Eu ≈ and Gd. TGA curves were used to determine the solvent content in the SUMOF-7II series (Figure 2.11(b)).

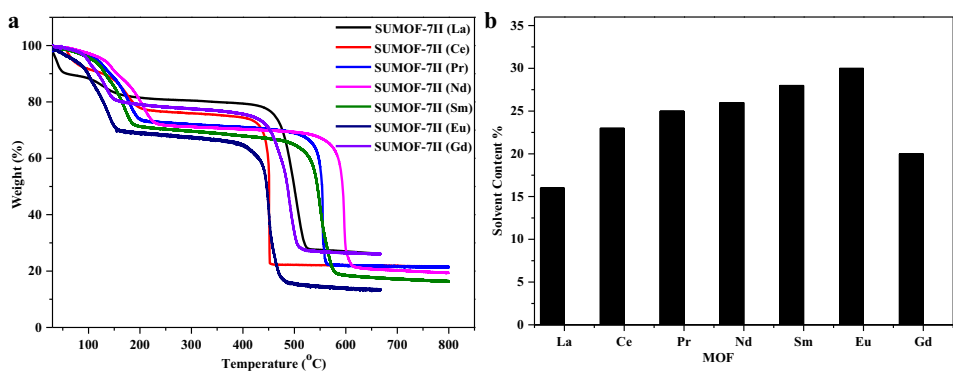


Figure 2.11. a) TGA analysis of isostructural lanthanides SUMOF-7II and b) the solvent content (weight loss at $T < 200$ °C). Figure reprinted from Paper II.

3. Synthesis of highly stable isoreticular lanthanide MOFs (SUMOF-7) with tunable luminescence properties and their sensing applications (Paper I-III)

3.1 Introduction

Lanthanide ions tend to have high coordination numbers^{107,108}. They form stable MOFs. Lanthanide clusters have unique physicochemical properties such as atomic magnetic moment³⁶. They also show remarkable photophysical properties such as luminescence⁵¹. Thus, they have been applied for sensing, biosensing, and light harvesting^{50,51}.

In our group, Yao et al. reported the synthesis of a mesoporous MOFs [$\text{Cu}_3(\text{L}2)_2(\text{H}_2\text{O})_3$] (denoted SUMOF-5) using a tritopic linker of pyridine-2,4,6-tribenzoic acid ($\text{H}_3\text{L}2$) and Cu as the metal clusters⁹². The material is stable for organic solvents such as DMF, CH_2Cl_2 , and EtOH. However, the dicopper paddle-wheel SBU [$\text{Cu}_2(\text{OOC})_4(\text{H}_2\text{O})_2$] in SUMOF-5 lacks stability in the presence of water molecules and under acidic or basic conditions. The low stability of SUMOF-5 limits its applications. Thus, the lanthanide clusters were selected to create stable MOF using the same organic linker.

In this chapter, a new series of isoreticular MOFs based on tritopic linkers and lanthanide elements are presented (SUMOF-7, Paper I). The photophysical properties of a selected tritopic linker ($\text{H}_3\text{L}2$, SUMOF-7II) are described using lanthanide clusters of La, Ce, Pr, Nd, Sm, Eu, Gd, Ho and Er (Paper II). The sensing and biosensing applications of SUMOF-7II (La) are demonstrated (Paper III). The SUMOF-7 series show several advantages such as high thermal and chemical stability. They offer excellent photophysical properties. The SUMOF-7II (La) serves as a sensitive probe for sensing and biosensing applications of ferric ions and tryptophan, respectively. The lanthanide metal clusters play a significant role in the material photophysical properties.

3.2. Synthesis of highly stable isoreticular lanthanide MOFs (SUMOF-7, Paper I)

Four organic linkers with different sizes (H_3L1 , H_3L2 , H_3L3 , and H_3L4) were used for the synthesis of SUMOF-7I to -7IV (Figure 3.1 & 3.2)⁴². The lanthanide metals clusters were La, Ce, Pr, Nd, Sm, Eu and Gd. The SUMOF-7 series have one-dimensional channels with the pore diameter from 8.4 to 23.9 Å⁴². They show permanent porosity and exhibit exceptionally high thermal and chemical stability (Figure 3.3)⁴².

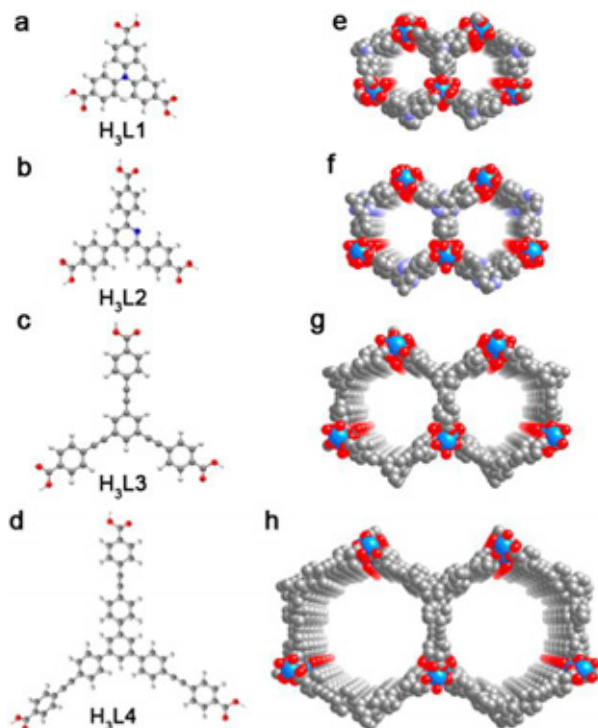


Figure 3.1. (a–d) Structures of the tritopic organic linkers that were used in the synthesis of SUMOF-7I to -7IV; H_3L1 (a), H_3L2 (b), H_3L3 (c), and H_3L4 (d), respectively, and (e–h) are the crystal structures of SUMOF-7I (e), SUMOF-7II (f), SUMOF-7III (g), and SUMOF-7IV (h). The diameters of the corresponding pore apertures are 8.4, 11.3, 16.3, and 23.9 Å, respectively (taking into account the van der Waals radii of the atoms)⁴². Figure reprinted with permission from Ref.⁴² (Paper I).

The SUMOF-7 series were synthesized using a hydrothermal method (85 °C, 16 h). SUMOF-7II (using the organic linker H₃L2, Figure 3.4) was synthesized using lanthanide elements of La, Ce, Pr, Nd, Sm, Eu, Gd, Ho, and Er. The mixed linkers of H₃L2 and 1,3,5-tris(4-carboxyphenyl)benzene (H₃BTB) were also used to synthesize lanthanides MOFs which are isostructural to SUMOF-7II (denoted SUMOF-7IIB, Figure 3.4). The ratio of the two linkers was determined using NMR. The ratios of H₃BTB:H₃L2 are ~1:1.

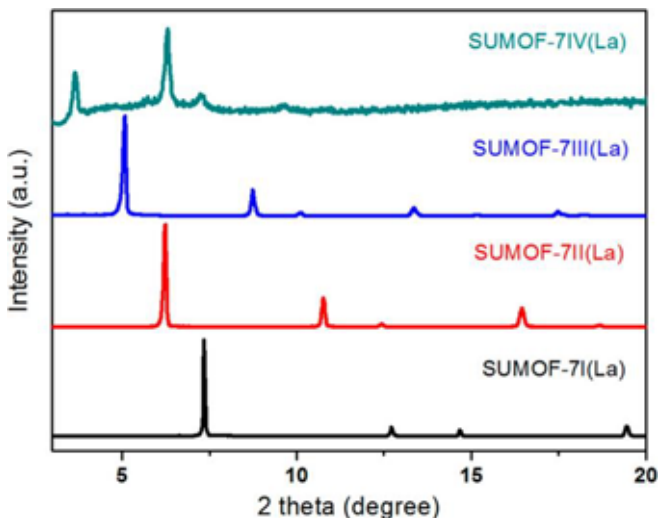


Figure 3.2. PXRD patterns of SUMOF-7I to -7IV (La). Figure reprinted with permission from Ref.⁴² (Paper I).

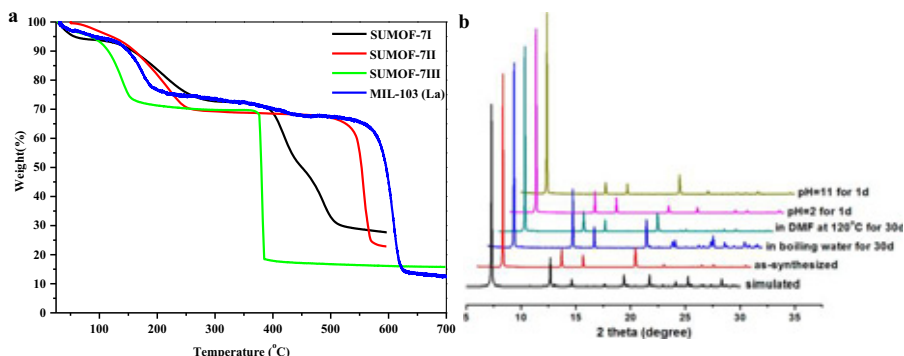


Figure 3.3. a) Thermal stability of SUMOF-7 using TGA and b) chemical stability using PXRD patterns under different conditions. Figure reprinted with permission from Ref.⁴² (Paper I).

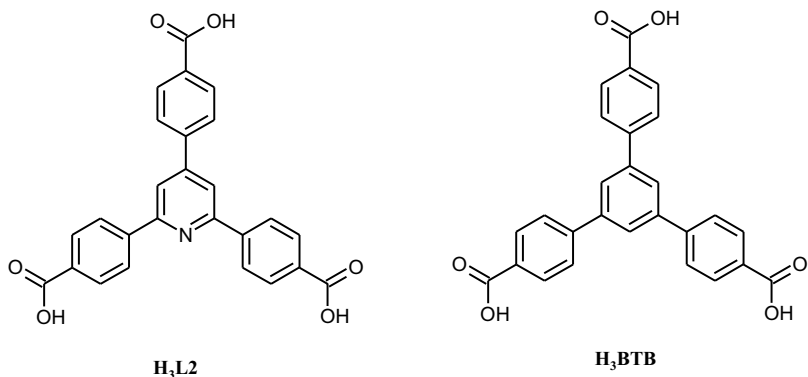


Figure 3.4. Chemical structure of the tritopic linker a) H₃L2 and b) H₃BTB.

3.3. Characterization of SUMOF-7II

SUMOF-7II and SUMOF-7IIB were characterized using PXRD (Figure 3.5). PXRD patterns show good agreement between the simulated and experimental pattern (Figure 3.5).

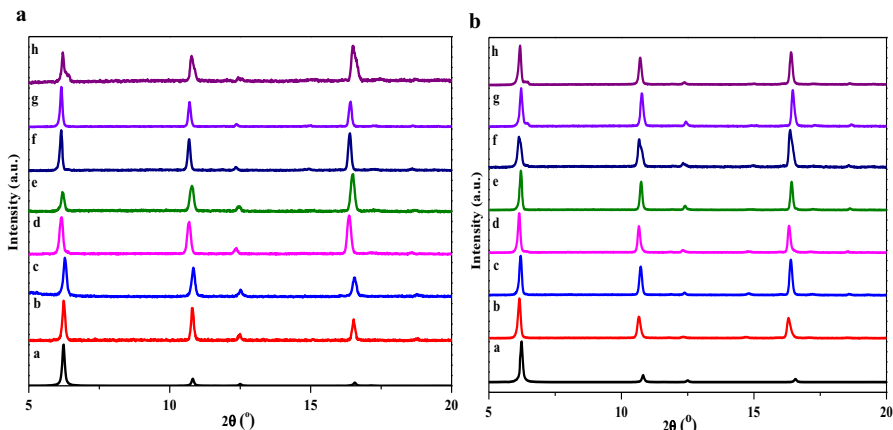


Figure 3.5. PXRD patterns of a) SUMOF-7II and b) SUMOF-7IIB for metal clusters of a) La, b) Ce, c) Pr, d) Nd, e) Sm, f) Eu and g) Gd. Figure reprinted from Paper II.

The chemical bonds in SUMOF-7II were confirmed using FT-IR (Figure 3.6). The free linker of H₃BTB or H₃L2 shows peaks at ~ 1710 cm^{-1} corresponding to C=O (Figure 3.6). After the coordination of the organic linker with lanthanide clusters, the free carbonyl group shows two peaks at ~ 1554 and 1364 cm^{-1} that are assigned as asymmetric

($\nu_a(\text{COO})$) and symmetric ($\nu_s(\text{COO})$) stretching, respectively¹⁰⁹. The peak at 470-480 cm⁻¹ is assigned as Ln—O. The absence of peaks at 1227 cm⁻¹ referring to C—O—H confirms that the materials are free from the unreacted linker. The morphology of the materials is rods with trigonal ends (Figure 3.7).

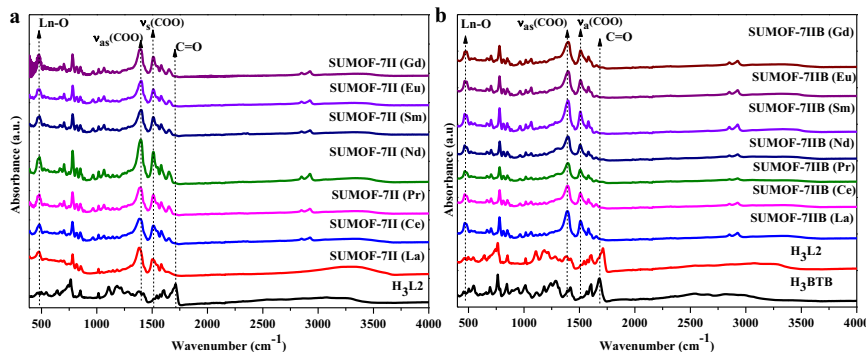


Figure 3.6. FT-IR spectra of a) SUMOF-7II and b) SUMOF-7IIB. Figure reprinted from Paper II.

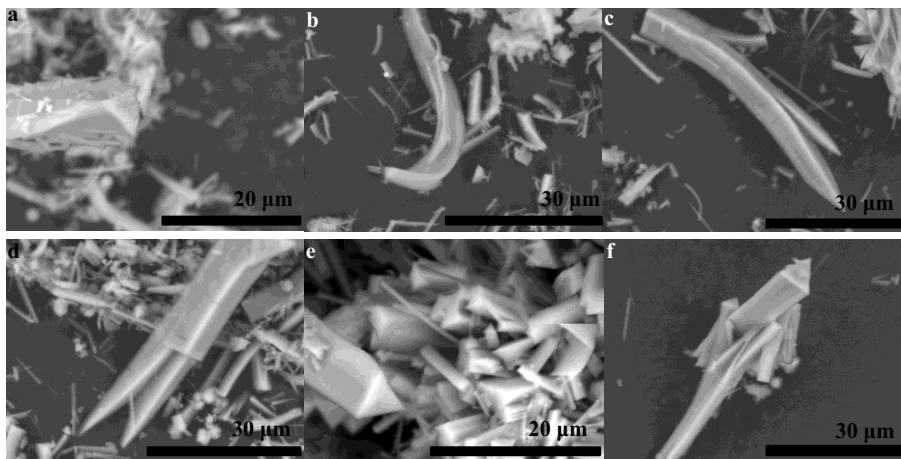


Figure 3.7. SEM images of SUMOF-7IIB for a) La, b) Ce, c) Pr, d) Nd, e) Sm, and f) Gd. Figure reprinted from Paper II.

3.4. Luminescence properties of SUMOF-7II (Paper II)

The isoreticular series of lanthanide MOFs (Ln-MOFs, SUMOF-7) show potential luminescence properties⁴². The organic linker H₃L2 sensitizes the lanthanide metal center through energy transfer from

non-bonding n electrons or π -conjugated organic chromophores to the Ln clusters. This process is known as "antenna effect". The carboxylic linker H₃L2 has a high binding tendency toward Ln³⁺ ions and serves as a potential sensitizer for Ln³⁺ clusters.

The antenna effect depends on the ligand and the metal properties¹¹⁰. The presence of pyridine moiety offers H₃L2 electron rich linker. H₃L2 shows two excitation peaks at 356 nm (E_g of 3.48 eV, 28 000 cm⁻¹) and 475 nm (E_g of 2.61 eV, 21 052 cm⁻¹, Figure 3.8(a)). H₃BTB shows only excitation at 325 nm (E_g of 3.81 eV, 30 769 cm⁻¹, Figure 3.8 (b)). The difference in the optical properties between H₃L2 compared to H₃BTB is due to the presence of the non-bonding "n" electrons of N center of pyridine ring in H₃L2.

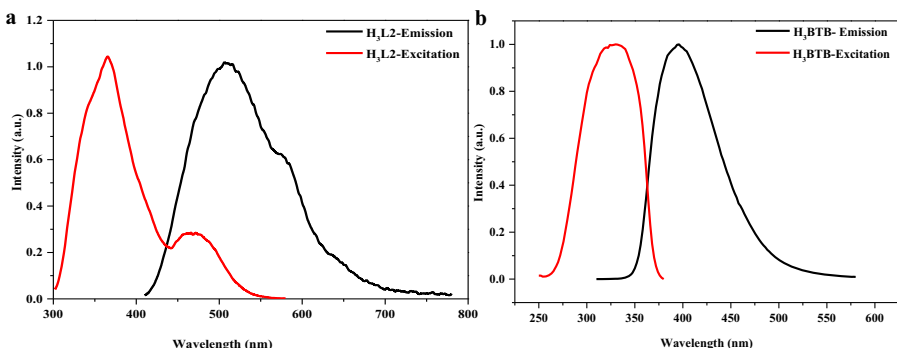


Figure 3.8. Excitation-emission for a) H₃L2 and b) H₃BTB. Figure reprinted from Paper II.

The electron transitions of the lanthanide MOFs can be 1) sharp intraconfigurational 4f–4f transitions of the electrons within the 4fⁿ subshell, 2) broad 4f–5d transitions: when a 4f electron excites to an empty 5d orbital, and 3) a broad charge transfer (CT) transition: in which one electron is transferred from the metal ion to the ligand (metal-to-ligand CT, MLCT) or vice versa (ligand-to-metal CT, LMCT)¹¹¹. In general, except for La³⁺ (f⁰) and Ce³⁺ (f¹), Ln³⁺ shows bands of excitation-emission that are originated from internal f-f electronic transitions¹¹². Interconfigurational 4fⁿ–4fⁿ⁻¹ transitions usually occur at energies higher than 33 000 cm⁻¹ (< 300 nm)¹¹¹.

The excitation-emission spectra of SUMOF-7II and SUMOF-7IIB of Eu clusters are shown in Figure 3.9. The f-f transitions of Eu clusters are noticed demonstrating that there is energy transfer from the ligand to the Eu³⁺ clusters. The major peaks at 580, 594, 619, 652 and 702 nm arise from the characteristic emission of the $^5D_0 \rightarrow ^7F_J$ ($J = 0-4$) transitions (Figure 3.9). The most intense emission at 619 nm is

attributed to the electric dipole-induced $^5D_0 \rightarrow ^7F_2$ (Figure 3.9). This transition is hypersensitive to the coordination environment surrounding the Eu³⁺ clusters. The second intense emission at 594 nm corresponds to the magnetic dipole-induced $^5D_0 \rightarrow ^7F_1$ transition. The intensity ratio of $^5D_0 \rightarrow ^7F_2$ to $^5D_0 \rightarrow ^7F_1$ is very sensitive to the structural change of Eu³⁺ clusters¹¹³. The ratios of the two peaks are 1:0.11 and 1:0.23 for SUMOF-7II and SUMOF-7IIB (Eu), respectively. SUMOF-7II (Eu) and SUMOF-7IIB (Eu) have quantum yields 3.65 and 5.08%, respectively.

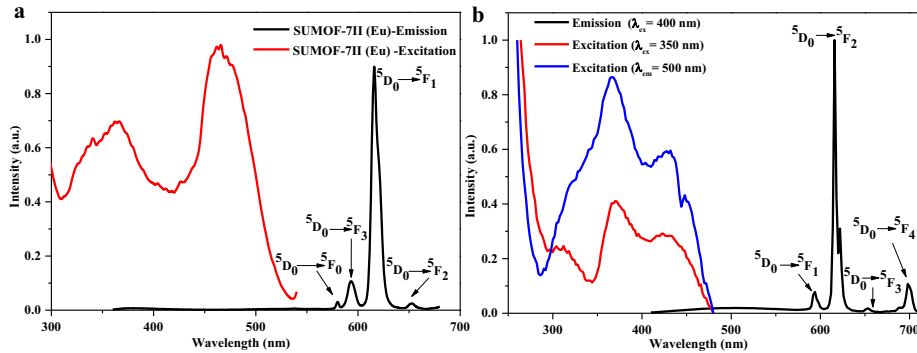


Figure 3.9. Excitation-emission of a) SUMOF-7II (Eu) and b) SUMOF-7IIB (Eu). Figure reprinted from Paper II.

Lanthanide Pr³⁺, Nd³⁺, Ho³⁺ and Er³⁺ display near infrared luminescence properties (Figure 3.10). Upon excitation at 350 nm, SUMOF-7II (Pr) displays bands with maxima at 1027 and 1475 nm, corresponding to $^1D_2 \rightarrow ^3F_{3,4}$ and $^1D_2 \rightarrow ^1G_4$ transitions of the Pr³⁺ clusters (Figure 3.10). SUMOF-7II (Nd) shows maxima emission peaks at 1060 and 1333 nm, which can be ascribed to $^4F_{3/2} \rightarrow ^4I_{11/2}$ and $^4F_{3/2} \rightarrow ^4I_{13/2}$ transitions of the Nd³⁺ clusters (Figure 3.10). SUMOF-7II (Ho) shows three bands at 980, 1180 and 1475 nm corresponding to $^5F_5 \rightarrow ^5I_7$, $^5I_6 \rightarrow ^5I_8$ and $^5F_5 \rightarrow ^5I_6$ transitions of the Ho³⁺ ions, respectively (Figure 3.10). SUMOF-7II (Er) demonstrates a broad band at 1535 nm with three shoulders (1500, 1560 and 1600 nm), which can be attributed to the $^4I_{13/2} \rightarrow ^4I_{15/2}$ transition of the Er³⁺ clusters (Figure 3.10). These observations indicate that H₃L2 sensitize NIR lanthanide elements.

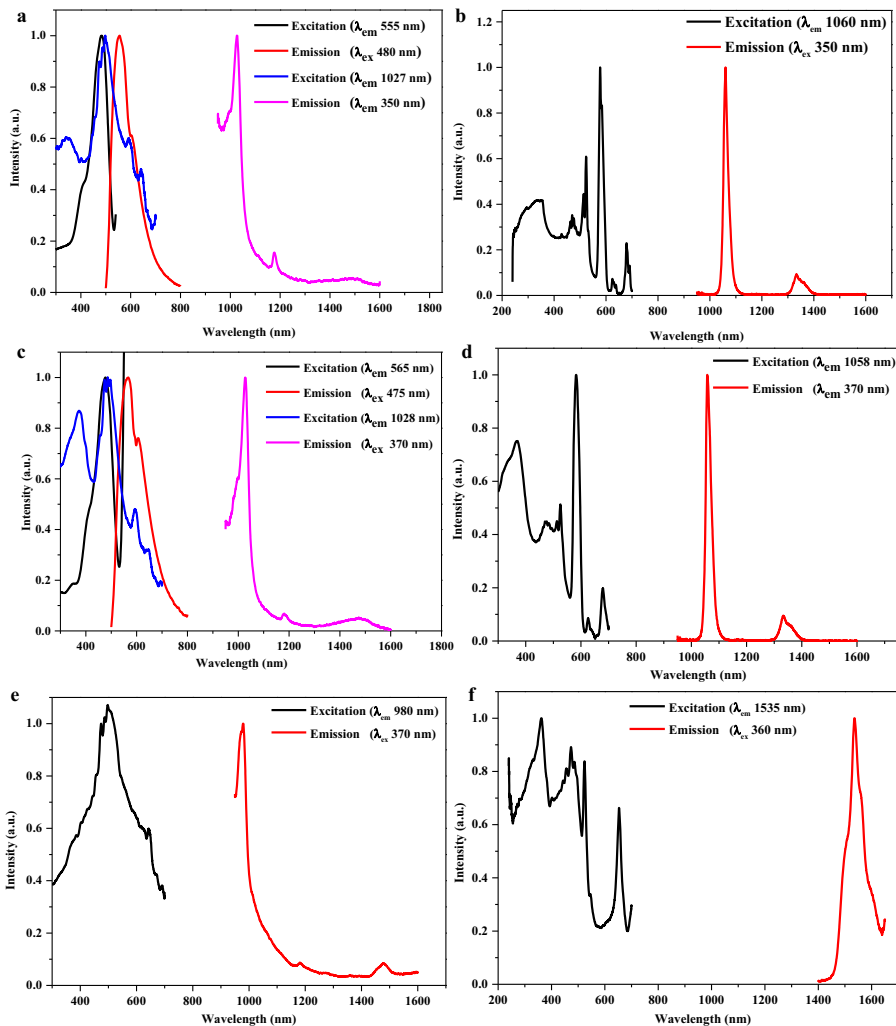


Figure 3.10 Excitation-emission of NIR lanthanide SUMOF-7II for a) SUMOF-7II (Pr), b) SUMOF-7II (Nd), c) SUMOF-7IIB (Pr), d) SUMOF-7IIB (Nd), e) SUMOF-7II (Ho), and f) SUMOF-7II (Er). Figure reprinted from Paper II.

3.5. Emission lifetime measurements using ultrafast spectroscopy

MOFs with long emission lifetime are good for applications including sensing, and biosensing. The long lifetime boosts time discrimination of the analyte and improves the signal-to-noise ratio¹¹⁴. The organic linker ($\text{H}_3\text{L}2$) shows a singlet state lifetime of 800 ps (Figure 3.11). The lifetimes of all SUMOF-7II are shorter than the lifetime of the

organic linker (800 ps, Figure 3.11). The decrease of the singlet lifetime is due to the antenna effect. The first lanthanide row covers the entire spectrum, from UV (Gd^{3+}) to visible (e.g. Pr^{3+} , Sm^{3+} , Eu^{3+} , Tb^{3+} , Dy^{3+} , and Tm^{3+}) and near infrared (NIR, e.g. Pr^{3+} , Nd^{3+} , Ho^{3+} , Er^{3+} , and Yb^{3+})¹¹¹. Some of these ions show simultaneous visible and NIR emitters (e.g. Pr^{3+} , Sm^{3+} , Eu^{3+} , Ho^{3+} , Er^{3+} , and Tm^{3+})¹¹¹. Data show that the emission lifetime of H₃L2 can be tuned using metal clusters. The near infrared elements such as Pr^{3+} and Nd^{3+} show the lowest emission lifetime. The emission lifetimes of SUMOF-7IIB are higher than those of SUMOF-7II for the same metal clusters. The increase of the lifetime is due to the presence of H₃BTB.

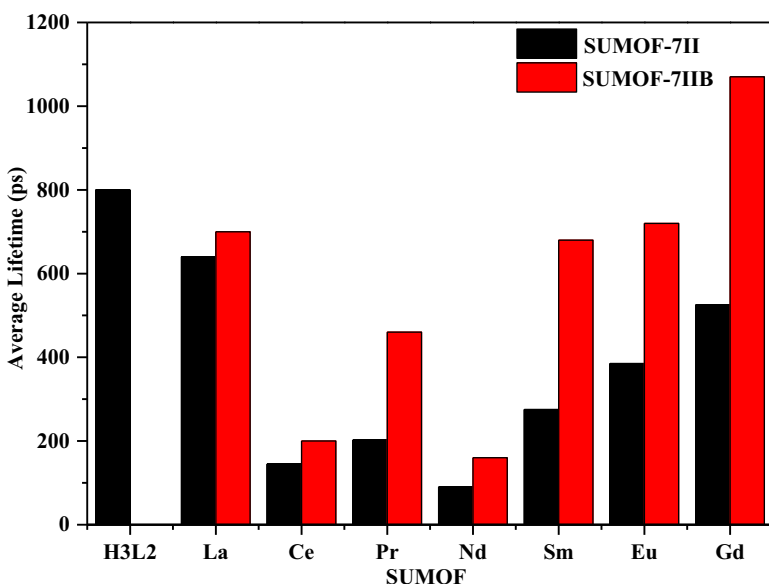


Figure 3.11. Lifetimes of SUMOF-7II and SUMOF-7IIB. Figure reprinted from Paper II.

3.6. Effect of the desolvation on the emission of SUMOF-7II (La and Eu)

The presence of solvent molecules in the pore of lanthanide MOFs influences the materials emission. SUMOF-7II series was synthesized in a mixed solvent of DMF, cyclohexanol, and water. It was reported that cyclohexanol fills the hexagonal pore of MIL-103 series that is isostructural to SUMOF-7II¹¹⁵.

Table 1. Photophysical properties of the linkers and SUMOF-7IIs. Data adapted from Paper II.

| Fluorophore | Ln^{3+} | G | E | F | τ (ps) | λ_{ex} (nm) | λ_{em} (nm) |
|-------------------|-----------------------------------|--------------------------------|--------------------------------|--|-------------|----------------------------|----------------------------|
| H ₃ L2 | | n, π | π* | π | 800 | 365, 475 | 510 |
| SUMOF-7II (La) | [Xe] | | π* | π | 640 | 365, 475 | 385, 525 |
| SUMOF-7II (Ce) | [Xe] ⁴ f ₁ | ² F _{5/2} | 5d | ² F _{5/2} | 145 | 325 | 400, 520 |
| SUMOF-7II (Pr) | [Xe] ⁴ f ₂ | ³ H ₄ | ¹ D ₂ | ³ F _{3,4} , ¹ G ₄ | 202 | 350 | 1027, 1475 |
| SUMOF-7II (Nd) | [Xe] ⁴ f ₃ | ⁴ I _{9/2} | ⁴ F _{3/2} | ⁴ I _{11/2} ⁴ I _{13/2} | 90 | 350 | 1060 1333 |
| SUMOF-7II (Sm) | [Xe] ⁴ f ₅ | ⁶ H _{5/2} | π* | π | 275 | 365, 470 | 380, 550 |
| SUMOF-7II (Eu) | [Xe] ⁴ f ₆ | ⁷ F ₀ | ⁵ D ₀ | ⁷ F ₀₋₆ | 385 | 365, 475 | 578- 695 |
| SUMOF-7II (Gd) | [Xe] ⁴ f ₇ | ⁸ S _{7/2} | π* | π | 525 | 350, 475 | 385, 520 |
| SUMOF-7II (Ho) | [Xe] ⁴ f ₁₀ | ⁵ I ₈ | ⁵ F ₅ | ⁵ I ₇ ⁵ I ₈ ⁵ T ₆ ⁵ I ₆ | 116 | 370 | 980 1180 1475 |
| SUMOF-7II (Er) | [Xe] ⁴ f ₁₁ | ⁴ I _{15/2} | ⁴ I _{13/2} | ⁴ I _{15/2} | 90 | 360 | 1535 |

Notes: G, ground state; E, emission; F, final state; τ, lifetime.

The emissions of SUMOF-7II (La, Figure 3.12(a)) and Eu (Figure 3.12(b))) before and after removing the guest solvent molecules were recorded. The luminescence of SUMOF-7II (La) shows a small shift (0.06 eV) of the emission peak (Figure 3.12(a)). On the other hand, SUMOF-7II (Eu) shows significant quenching of ⁵D₀→⁷F_J (J = 0-4, Figure 3.12(b)). The same observation was reported for MIL-103 ($\text{Tb}_{0.95}\text{Eu}_{0.05}$)¹¹⁶. The changes of excitation-emission of the investigated samples are due to the overlap of the solvent molecules with the electronic state of SUMOF-7II (La, and Eu). These observations imply that the guest molecules influenced the fluorescence emission.

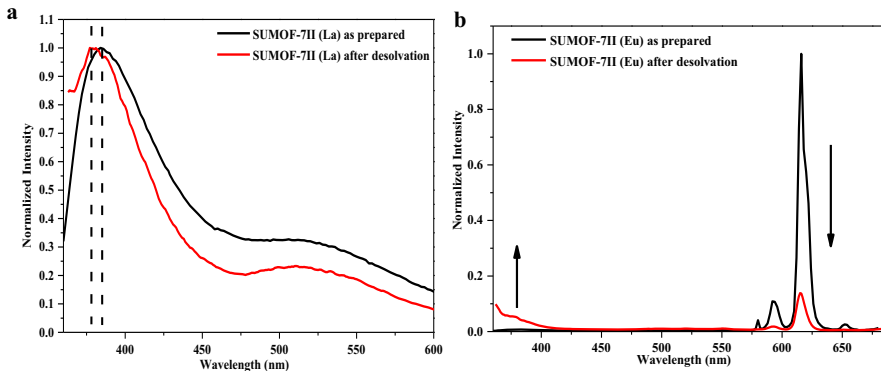


Figure 3.12. Emission of a) SUMOF-7II (La) and b) SUMOF-7II (Eu) before and after desolvation. Figure reprinted from Paper II.

3.7. Photostability

Photostability of SUMOF-7II (La, Eu, and Gd) was reported (Figure 3.13). Data show an excellent photostability for SUMOF-7II (Eu) and SUMOF-7II (Gd) (< 1% loss in the material emission) compared to the organic linker H₃L2 (-28%) and SUMOF-7II (La, -18%).

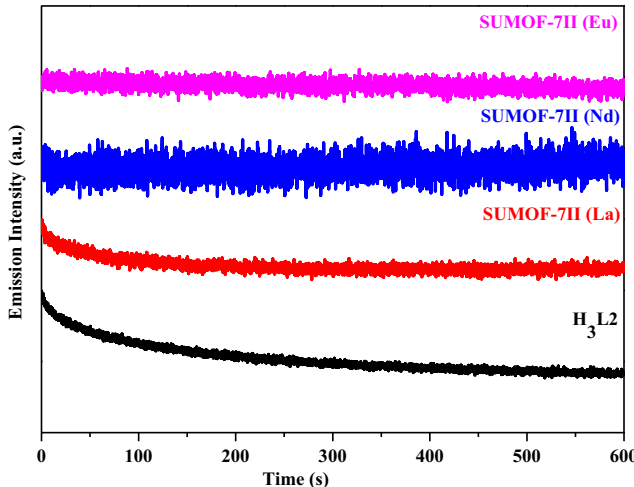


Figure 3.13. Photostability of SUMOF-7II under continuous light irradiation. Figure reprinted from Paper II.

3.8. Potential applications for SUMOF-7II

The properties of SUMOF-7II offer many potential applications. The pore size of SUMOF-7II (11.3 Å) provides accessibility for molecules

with size less than 1 nm. The materials are stable in water and can be applied for sensing of metal ions and biosensing. The magnetic properties of SUMOF-7II (Gd) may be useful as contrasting agents for magnetic resonance imaging (MRI).

3.9. Preparation of SUMOF-7II nanoparticles (Paper III)

SUMOF-7II (La) has high thermal and photostability. It was prepared as nanoparticles (average particle size of 60 nm) via grinding and dispersion in ethanol⁹⁴. The dispersion has high stability. SUMOF-7II (La) shows strong emission signal compared to the H₃L2 solution (Figure 3.14(a)).

3.10. Stability of SUMOF-II (La)

A dispersed solution of SUMOF-7II (La) shows no emission signal change over several months (Figure 3.14(b)). SUMOF-7II (La) shows stable emission signals over a pH range of 6-12 (Figure 3.14(c)). It shows negligible signal fluctuations for different batches (Figure 3.14(d)).

3.11. Sensing of ferric ions using SUMOF-7II (La)

Applications of SUMOF-7II for the detection of metal ions were investigated (Figure 3.15). Fe²⁺ and Fe³⁺ ions show selective quenching of the fluorescence emission signal of a dispersed SUMOF-7II (La) (Figure 3.15). The quenching of Fe²⁺ species could be due to the presence of Fe³⁺ impurities caused by auto-oxidation of Fe²⁺. SUMOF-7II (La) shows significant differences in response to different Fe³⁺ salts. Fe(AcO)₃ shows a higher quenching effect compared to FeCl₃ (Figure 3.15).

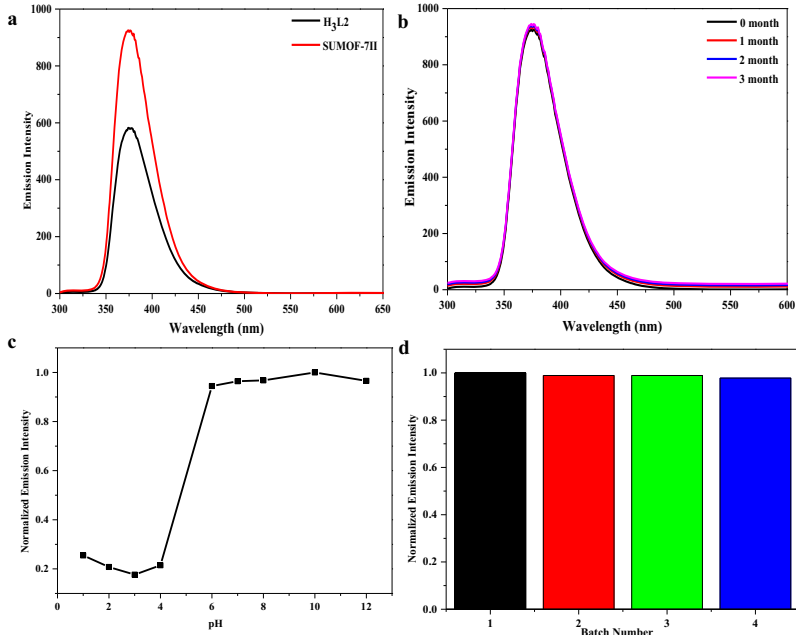


Figure 3.14 a) Emission spectra of $\text{H}_3\text{L}2$ and SUMOF-7II (La), b) emission of dispersed SUMOF-7II(La) over time, c) pH effect on the emission intensity and d) emission signal for different batches. Figure reprinted from Ref.⁹⁴ (Paper III).

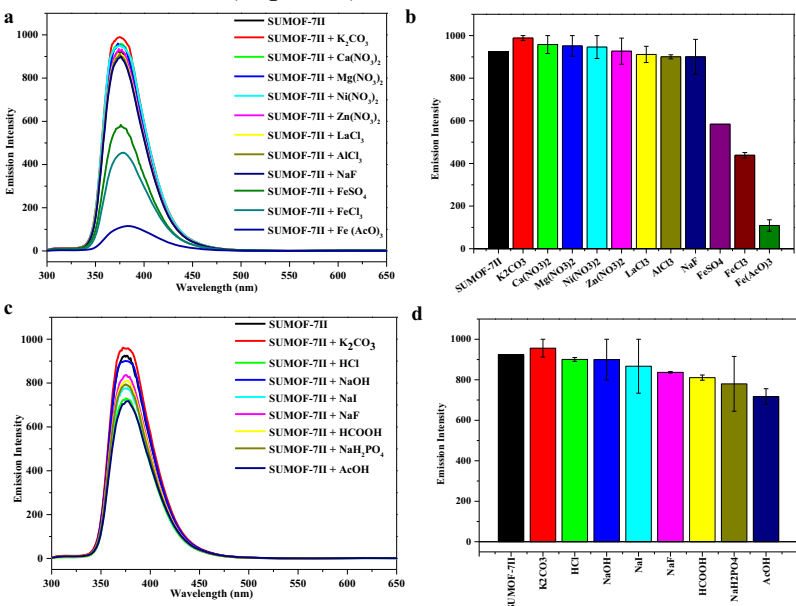


Figure 3.15. Emission of SUMOF-7II (La) upon interactions with different a-b) cations and b-d) anions. Figure reprinted from Ref.⁹⁴ (Paper III).

The quantitative analysis of Fe^{3+} (FeCl_3 and $\text{Fe}(\text{AcO})_3$) using SUMOF-7II as a probe was investigated (Figures 3.16). The emission of SUMOF-7II decreases with the increase of the Fe^{3+} concentration (Figure 3.16). The signal shows a linear relationship with the concentration of Fe^{3+} in the range of 0–167 μM . The Stern-Volmer quenching constant (K_{sv}) ($I_0/I = 1 + K_{\text{sv}}[Q]$, where $[Q]$ represents the Fe^{3+} concentration), is $4.3 \times 10^3 \text{ M}^{-1}$ for $\text{Fe}(\text{AcO})_3$ and $2.1 \times 10^4 \text{ M}^{-1}$ for FeCl_3 . These values indicate that Fe^{3+} ions have a high quenching capability due to the dynamical quenching. Also, the fluorescence response of SUMOF-7II to Fe^{3+} is speedy (< 2 min), which is more than five times faster than that reported using MIL-53 (Al) (> 10 min)¹⁷.

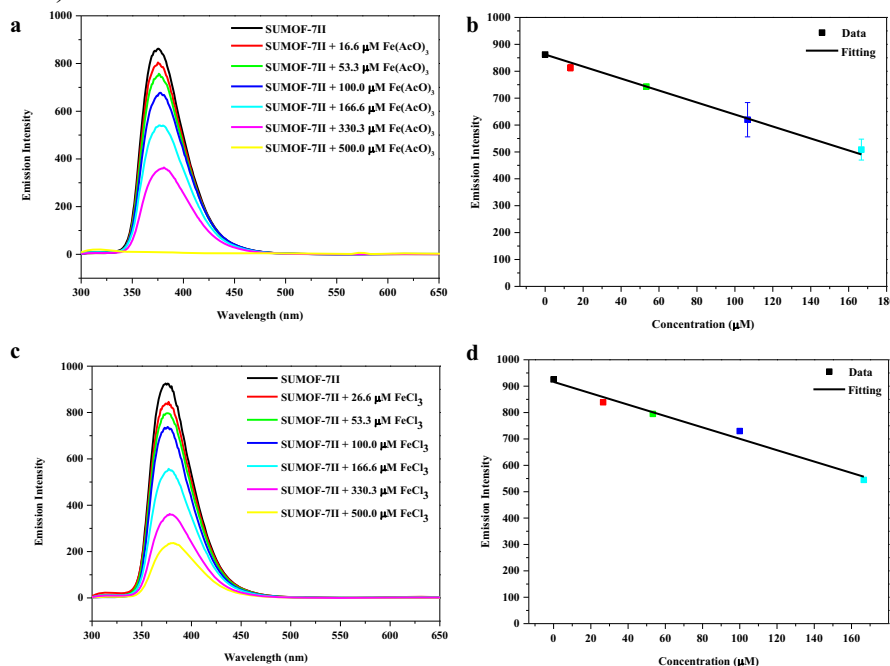


Figure 3.16 Fluorescence response of SUMOF-7II upon addition of $\text{Fe}(\text{AcO})_3$ (a) and FeCl_3 (c) at pH 7.4 ($\lambda_{\text{ex}} = 285 \text{ nm}$), and as a function of the Fe^{3+} concentration for $\text{Fe}(\text{AcO})_3$ (b) and FeCl_3 (d). Figure reprinted from Ref.⁹⁴ (Paper III).

3.12. Characterization of interactions between SUMOF-7II and Fe (III)

The interactions of SUMOF-7II with Fe^{3+} ions were investigated using PXRD, EXAFS, and FT-IR (Figure 3.17). PXRD patterns show that

the crystallinity of SUMOF-7II is retained in the presence of Fe^{3+} (FeCl_3 and $\text{Fe}(\text{AcO})_3$, Figure 3.17(a)). XAS shows that Fe K -edge (7.112 keV) of FeCl_3 and $\text{FeCl}_3@\text{SUMOF-7II}$ are the same (Figure 3.17(b)). This observation reveals that there is no change of the oxidation state of Fe^{3+} . A stronger interaction of $\text{Fe}(\text{AcO})_3$ with SUMOF-7II is observed from the FT-IR spectra (Figure 3.17(c)), showing that $\text{Fe}(\text{AcO})_3$ play a significant role in the quenching of SUMOF-7II emission compared to other Fe^{3+} species. The peaks at 2990 and 1100 cm^{-1} refer to C—H and C—O from acetate and SUMOF-7II, respectively. The La—O peak is shifted from 480 to 450 cm^{-1} in the presence of acetate ions (AcO^- , Figure 3.17(c)). The splitting of $(\text{COO})_{\text{as}}$ indicates that acetate (AcO^-) ions coordinate to the framework metal La^{3+} .

SUMOF-7II and $\text{Fe}^{3+}@\text{SUMOF-7II}$ show higher thermal stability (> 500 °C) compared to the organic linker $\text{H}_3\text{L}2$ (200 °C, Figure 3.17(d)).

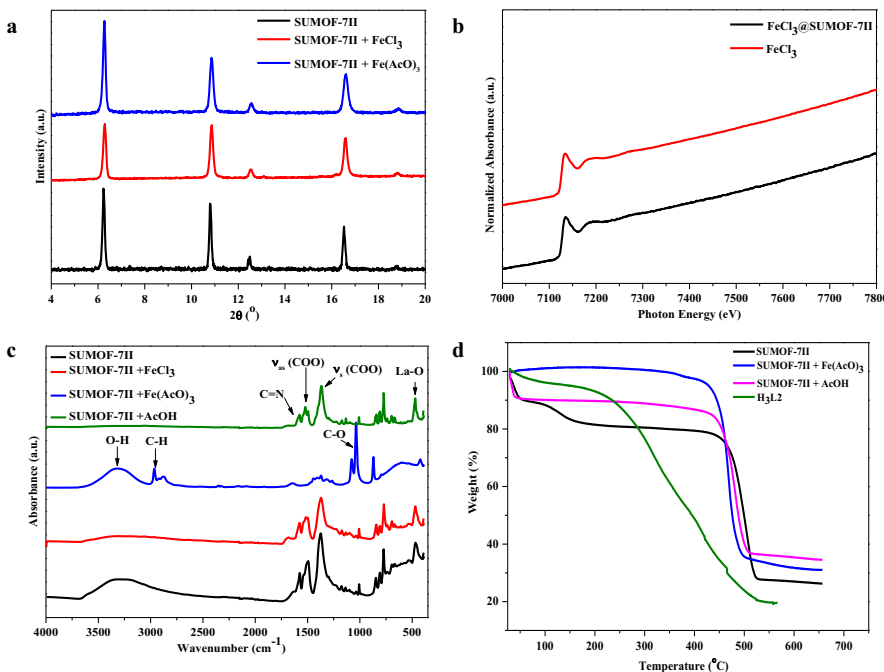


Figure 3.17 (a) PXRD of SUMOF-7II without and with FeCl_3 or $\text{Fe}(\text{AcO})_3$, (b) XAS spectra of Fe K -edge (E equal to 7112 eV) for $\text{FeCl}_3@\text{SUMOF-7II}$ and FeCl_3 , (c) FT-IR of SUMOF-7II with AcOH, FeCl_3 and $\text{Fe}(\text{AcO})_3$, and (d) TGA curves. Figure reprinted from Ref.⁹⁴ (Paper III).

3.13. Biosensing of tryptophan

The selectivity of SUMOF-7II towards selected amino acids of L-histidine, L-asparagine, L-glutamine, L-leucine, L-methionine, and L-tryptophan was tested (Figure 3.18). The absorbance wavelength matches of tryptophan and SUMOF-7II at 285 nm resulted in selective quenching of SUMOF-7II (Figure 3.18(a)). The fluorescence emission of SUMOF-7II shows a direct linear response with the concentration of tryptophan (Figure 3.18(b)). The Stern Volmer equation gives a K_{SV} constant of $1.69 \times 10^3 \text{ M}^{-1}$. The high selectivity of SUMOF-7II toward tryptophan is due to dynamic quenching and energy transfer.

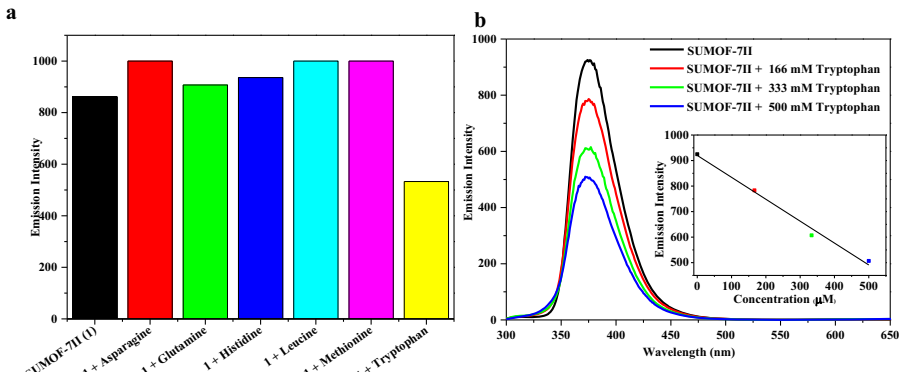


Figure 3.18 The fluorescence response of SUMOF-7II (a) in the presence of selected amino acids (0.166 mM) showing the selectivity of SUMOF-7II towards tryptophan and (b) at different concentrations of tryptophan. Figure reprinted from Ref. ⁹⁴ (Paper III).

4. One-pot encapsulation of dye/protein and synthesis of hierarchical porous ZIF-8 nanoparticles (Paper IV)

4.1. Introduction

ZIF-8 is a microporous material that consists of zinc as a metal center and 2-methyl imidazole (Hmim) as an organic linker¹¹⁹. ZIF-8 was used for many applications including carbon dioxide capture¹²⁰, hydrogen storage¹²¹, small molecule separation¹²¹, catalysis¹²², drug delivery⁴⁶ and batteries¹²³. ZIF-8 was synthesized using various methods including solvothermal method¹²⁴, CVD⁶⁸, and steam-assisted conversion⁷¹. It has micropores with largest cavity and pore opening of 11.4 and 3.4 Å, respectively. The small pore of ZIF-8 limits the mass diffusion and the material applications. Thus, several methods have been reported to synthesize hierarchical porous ZIF-8 (micropore and mesopore) using the templates of sodium dodecyl sulfate (SDS)¹²⁵, block co-oligomer micelles¹²⁶, organic compounds⁴⁶, and co-template of cetyl trimethyl ammonium bromide (CTAB) and L-histidine (His)¹²⁷.

In this chapter, a simple one-pot encapsulation of dye or protein and synthesis of hierarchical porous ZIF-8 at room temperature is described. The effect of the reaction parameters; such as reactants ratio, reaction time, TEA and dye/protein concentrations, were investigated. Ex situ X-ray diffraction shows that there is an *in-situ* formation of ZnO nano rice before the formation of hierarchical porous ZIF-8. The mesoporosity of ZIF-8 can be tuned in diverse ways including increasing the concentration of the dye or the base as well as post-synthetic treatment (reflux). The excitation-emission, lifetime, and photostability of the free dye and dye@ZIF-8 were investigated. Data shows the improvement of the photophysical properties of the encapsulated dye. The method has been applied to synthesize other ZIFs such as dye@ZIF-67 (Co-based ZIF).

4.2. Synthesis of ZIF-8

Schematic representation for the synthesis of dye encapsulated ZIF-8 is shown in Figure 4.1. The synthesis procedure is a one-pot method using TEA-assisted approach. TEA was first added to the solution of

$\text{Zn}(\text{NO}_3)_2$. A white precipitate of ZnO nano rice was observed. Then, a target dye of RhB, MB, or protein was added. Finally, the organic linker solution of 2-methylimidazole was added. The reaction solution was stirred for 30 min, and the precipitate was collected using centrifugation.

Dye@ZIF-67 was synthesized using the same procedure, but $\text{Co}(\text{NO}_3)_2$ was used as the metal salt instead of $\text{Zn}(\text{NO}_3)_2$.

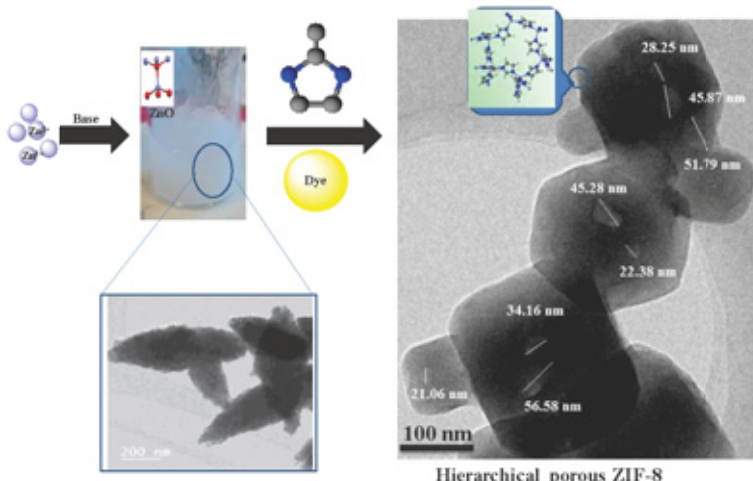


Figure 4.1. Schematic representation of dye encapsulation and formation of hierarchical porous ZIF-8. Figure reprinted with permission from Ref.⁹⁵ (Paper IV).

4.3. Characterization of ZIF-8

The PXRD pattern shows that the white precipitate formed after the addition of TEA to the solution of $\text{Zn}(\text{NO}_3)_2$ is ZnO (Figure 4.2 (a)). The reaction conditions including Hmim:Zn ratio, reaction time, TEA and dye/protein concentrations were optimized and monitored using PXRD (Figure 4.2). The PXRD patterns show that the materials can be synthesized using TEA of 0.7–14 mmol (Figure 4.2 (b)). The reactions were completed within 2 min (Figure 4.2 (a)). The material can be synthesized using a small ratio of Hmim:Zn of ~2 (Figure 4.2 (c)). The concentration of RhB up to 30 μmol shows no change of the material crystallinity (Figure 4.2 (d)).

The morphology and porosity of RhB@ZIF-8 using molar ratios of Hmim:Zn (2, 7, 10 and 24) was reported (Figure 4.3). At low molar ratio (Hmim:Zn of 2), spherical ZIF-8 nanoparticles were observed

(Figure 4.3). The average particle sizes of RhB@ZIF-8 decrease with the increase of Hmim:Zn molar ratios (Figure 4.3).

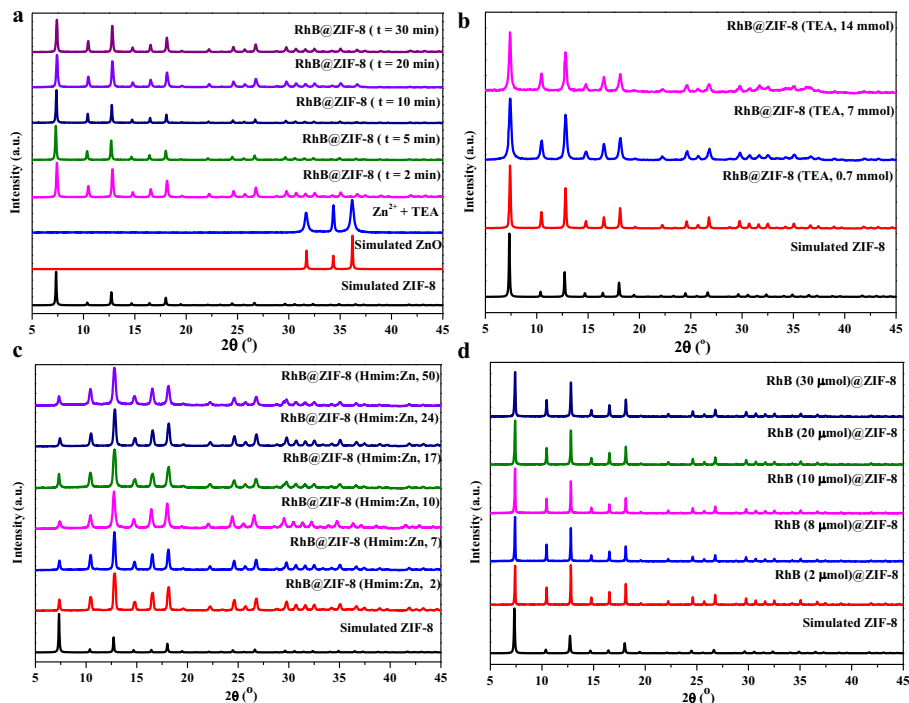


Figure 4.2. PXRD pattern of dye@ZIF-8 synthesized at a) different reaction time, and different concentrations of b) TEA, c) Hmim:Zn ratio and d) RhB loading. Figure reprinted with permission from Ref.⁹⁵ (Paper IV).

The chemical bonds and connectivity of RhB@ZIF-8 were confirmed using FT-IR spectroscopy (Figure 4.4). The absence of the peaks of both the bending at 1678 cm^{-1} and the stretching N—H vibration at 1581 cm^{-1} of Hmim indicates that the prepared materials have no free organic linker^{128,129}. The peak of Zn—N stretching around 420 cm^{-1} approves the coordination of the metal and the linker¹³⁰. This peak is very sensitive to the changes in the local structure of Zn nodes in ZIF-8.¹³¹ There is no noticeable change in the wavenumber of Zn—N stretching peak with and without the dye. This observation shows that there is no apparent interaction between the dye molecules and Zn nodes of the framework.

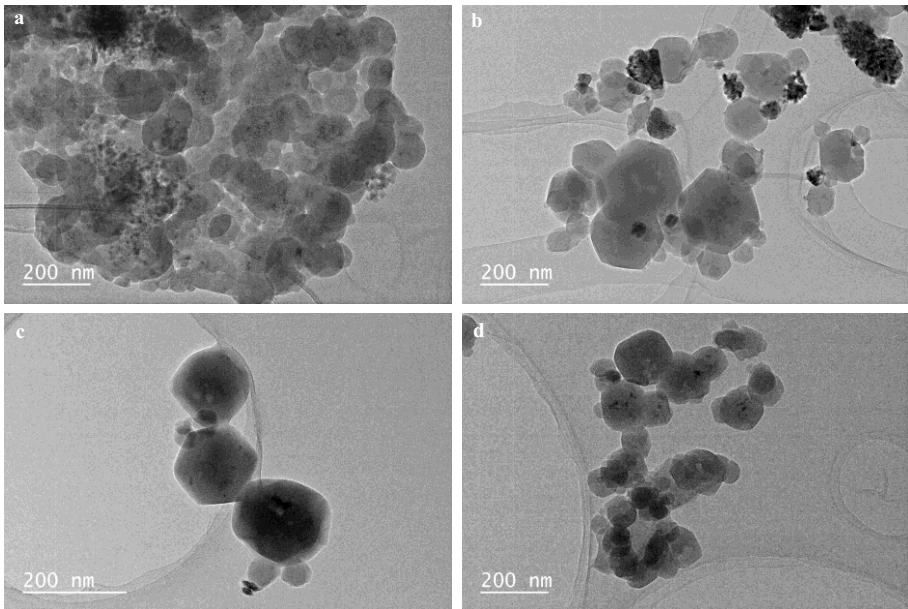


Figure 4.3. TEM images of ZIF-8 using a molar ratio of Hmim:Zn, a) 2, b) 7, c) 10, d) 24. Figure reprinted with permission from Ref.⁹⁵ (Paper IV).

The material porosity was characterized using N₂ adsorption (Figure 4.5, Table 4.1) and TEM (Figure 4.6). Data show that the prepared materials are hierarchical porous frameworks (Figure 4.5). The surface area of dye@ZIF-8 increases with the increase of the dye loadings, the amount of TEA, or reflux (Figure 4.5). The pore volume of the materials increases with the increase of the TEA concentration or reflux without change of the material crystallinity. NLDFT analysis shows broad pore size distribution (5-60 nm) with the maximum pore volume at 40 nm after reflux and 15-40 nm using high concentration of TEA (Figure 4.5). TEM images show pore size of ~20 nm (Figure 4.5). The presence of pore with the size of 22-59 nm was also observed (Figure 4.1). The pore size distribution and TEM images indicate that the synthesized ZIF-8 has a hierarchical porous structure.

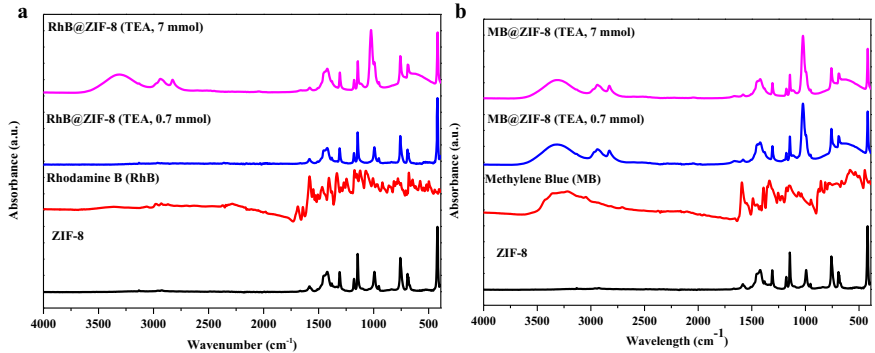


Figure 4.4. FT-IR spectra of RhB@ZIF-8 (a) and MB@ZIF-8 (b). Figure reprinted with permission from Ref.⁹⁵ (Paper IV).

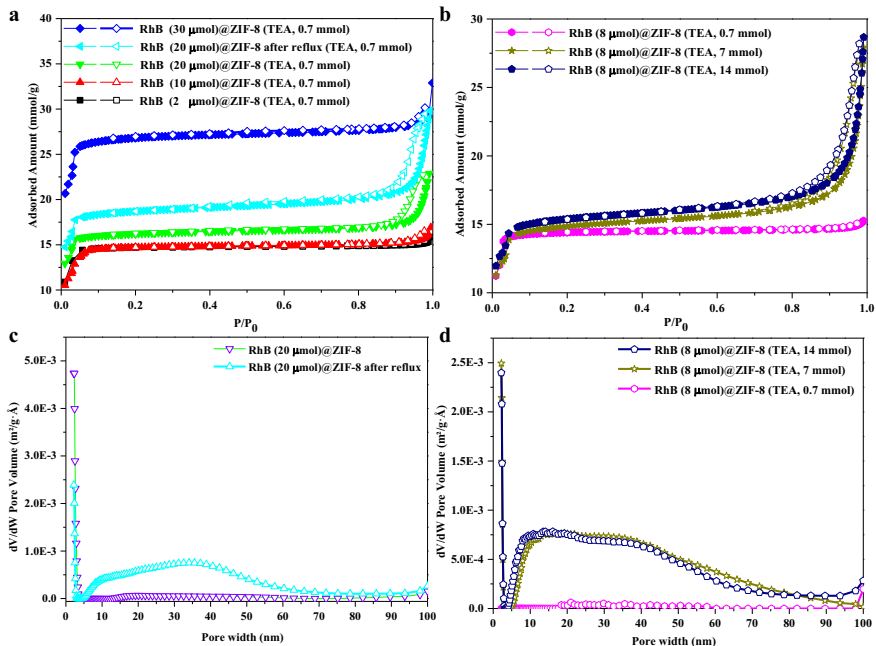


Figure 4.5. a-b) N_2 adsorption (closed symbol)-desorption (open symbol) isotherm for RhB@ZIF-8 using different concentrations of a) RhB and b) TEA, and c-d) pore size distribution using NLDFT method. Figure reprinted with permission from Ref.⁹⁵ (Paper IV).

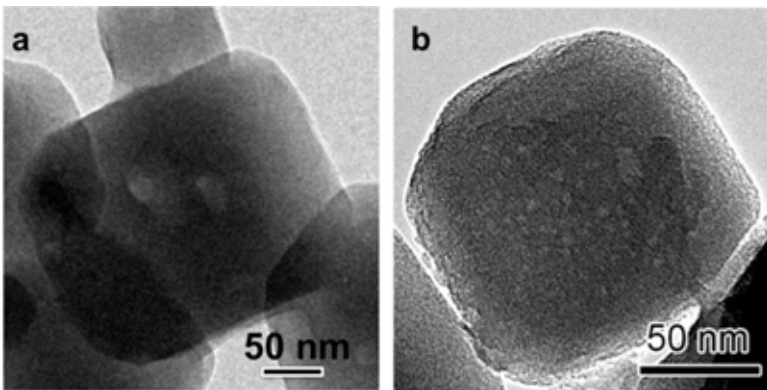


Figure 4.6. TEM images of RhB@ZIF-8 synthesized using (a) 0.7 mmol and (b) 14 mmol TEA. Figure reprinted with permission from Ref.⁹⁵ (Paper IV).

4.4. Photophysical properties of dye@ZIF-8

Photophysical properties of the dyes encapsulated into ZIF-8 were investigated using emission-excitation, and lifetime measurements (Figure 4.7). At an excitation wavelength of 500 nm, the fluorescence emission was observed at 620 and 575 nm for RhB and RhB@ZIF-8, respectively. The emission peak of RhB@ZIF-8 is narrower compared to the free dye (RhB). The dye encapsulation increases the dye rigidity and reduces the dye aggregation.

The emission lifetimes (τ) for RhB@ZIF-8 and MB@ZIF-8 are longer than those of the corresponding free dyes (Figure 4.7). The lifetime value increases with the increase of the TEA amount (Figure 4.7). The lifetime of the dyes after encapsulation is increased by several orders (2-27 folds for RhB and 20 folds for MB, Figure 4.7) that are due to the de-aggregation, deprotonation and increase the rigidity of the dye.

Table 4.1 Summary of the yield and N₂ adsorption analysis of hierarchical porous ZIF-8 using dyes and protein. Table reprinted with permission from Ref.⁹⁵ (Paper IV).

| Targe molecules (μmol) | TEA (mmol) | Yield (%) ^a | S _{BET} (m^2/g) | S _{Lan} (m^2/g) | Pore V ^b | V _{micro} | V _{meso} |
|-------------------------------------|------------|------------------------|--|--|---------------------|--------------------|-------------------|
| Rhodamine B | | | | | | | |
| 2 | 0.7 | 80 | 1344 | 1443 | 0.53 | 0.49 | 0.04 |
| 8 | | 79 | 1349 | 1416 | 0.52 | 0.47 | 0.05 |
| 10 | | 80 | 1384 | 1487 | 0.55 | 0.47 | 0.08 |
| 20 | | 47 | 1475 | 1601 | 0.75 | 0.51 | 0.24 |
| 20 (after reflux) | | 40 | 1718 | 1851 | 0.96 | 0.57 | 0.39 |
| 30 | | 22 | 2545 | 2684 | 1.00 | 0.83 | 0.17 |
| 8 | 7 | 62 | 1358 | 1515 | 0.87 | 0.45 | 0.42 |
| 8 | | 68 | 1360 | 1515 | 0.90 | 0.46 | 0.44 |
| 0 | | 60 | 983 | 1130 | 0.44 | 0.34 | 0.10 |
| Methylene Blue | | | | | | | |
| 20 | 0.7 | 63 | 1513 | 1612 | 0.61 | 0.55 | 0.06 |
| Bovine Serum Albumin | | | | | | | |
| 0.06 | 0.7 | 70 | 1612 | 1846 | 0.69 | 0.57 | 0.12 |

Notes: ^a The yield of dye@ZIF-8 was calculated based on Zn, ^b using single point adsorption at P/P₀ of 0.98. Volume (V) unit is cm³/g.

4.5. Photostability of the dye and dye@ZIF-8

The photostability measurements show that the encapsulated dye has lower photostability compared to the free dye (Figure 4.8). The decrease of the dye's photostability is due to the increase of the dye's rigidity.

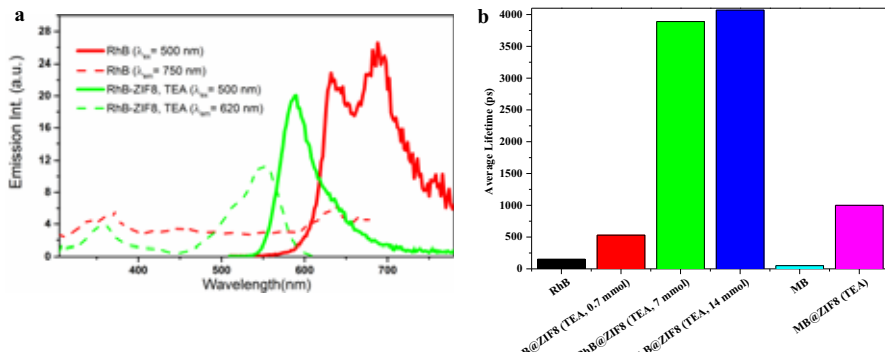


Figure 4.7. a) Excitation-emission and b) lifetime for dye and dye@ZIF-8. Figure reprinted with permission from Ref.⁹⁵ (Paper IV).

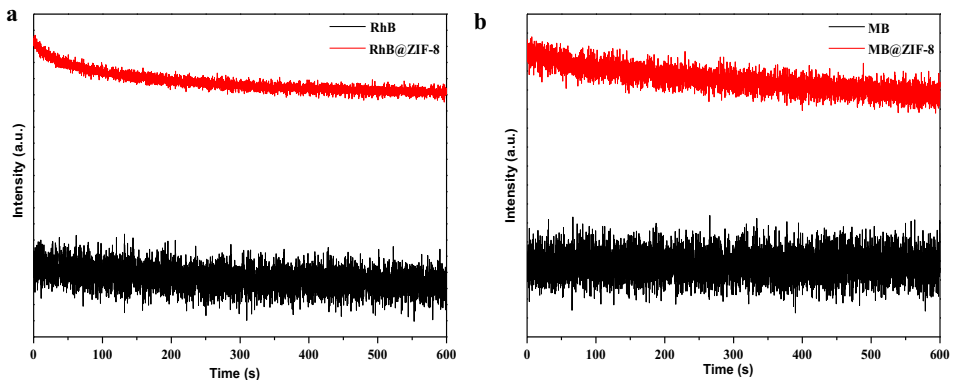


Figure 4.8. Photostability of a) RhB@ZIF-8 and b) MB@ZIF-8 under continuous irradiation. Figure reprinted with permission from Ref.⁹⁵ (Paper IV).

4.6. Encapsulation of a protein into ZIF-8 and the synthesis of dye@ZIF-67

The protein bovine serum albumin (BSA) encapsulated into ZIF-8 using the TEA-assisted approach shows no change in the PXRD patterns for the loading range of 1-4 mg BSA (Figure 4.9 (a)). TEM image (Figure 4.9 (b)) and N₂ adsorption (Figure 4.9 (c)) confirm the presence of mesoporosity. The tryptophan emission confirms the presence of BSA in the final product (Figure 4.9 (d)).

The synthesis of dye@ZIF-67 was also successfully achieved using the same procedure (Figure 4.10).

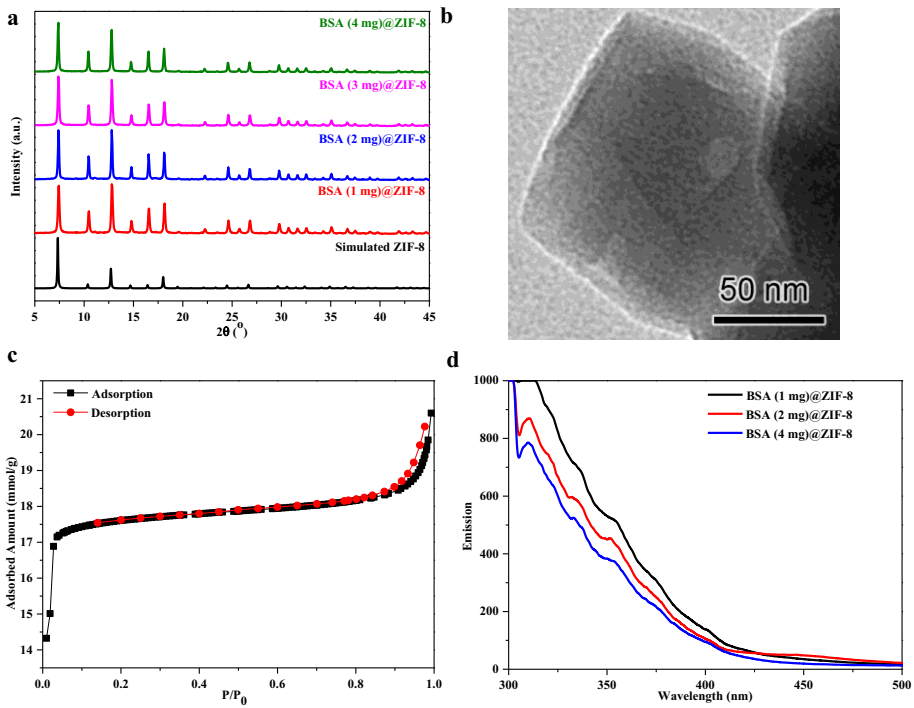


Figure 4.9. Characterization of BSA@ZIF-8 using a) PXRD, b) TEM, c) N_2 adsorption isotherm and d) fluorescence spectroscopy. Figure reprinted with permission from Ref.⁹⁵ (Paper IV).

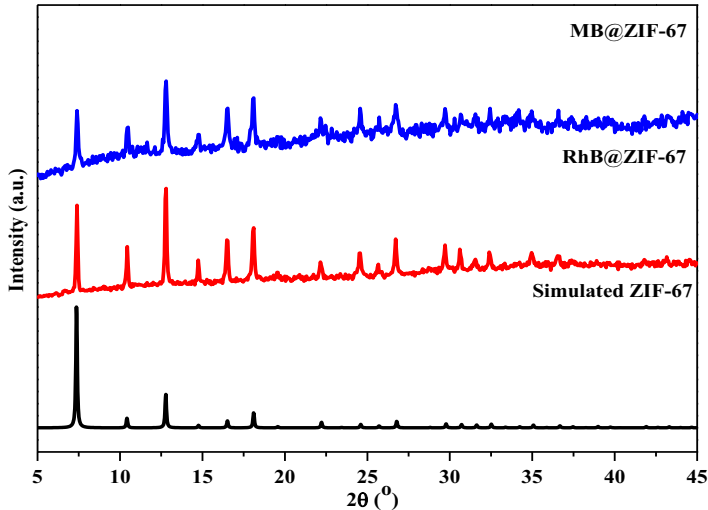


Figure 4.10. PXRD patterns of dye@ZIF-67. Figure reprinted with permission from Ref.⁹⁵ (Paper IV).

5. Template-free and room temperature synthesis of hierarchical porous zeolitic imidazole framework nanoparticles and their CO₂ sorption (Paper V)

5.1. Introduction

Hierarchical porous ZIF-8 was synthesized using the template based methods including enzyme¹³², organic molecules⁴⁶, and other template molecules^{133,134}. These methods require template molecules, tedious synthesis procedure, and an extra step to remove the template molecules^{135,136}.

In this chapter, a template-free approach for the synthesis of hierarchical porous ZIF-8 is described. The formation of zinc hydroxide nitrate nanosheets after the addition of certain concentration of sodium hydroxide leads to the formation of hierarchical porous ZIF-8 without organic template. The method can be applied for the synthesis of ZIF layers (ZIF-L).

5.2. Synthesis of hierarchical porous ZIF-8 using template-free approach

Sodium hydroxide solution (0.02-3 mmol) was added to the solution of $\text{Zn}(\text{NO}_3)_2 \cdot 6\text{H}_2\text{O}$. White precipitates of zinc hydroxy nitrates or ZnO nanosheets were observed. Then, the solution of Hmim was added, and the reaction mixture was stirred for one hour at room temperature. The product was collected using centrifugation. The same protocol was applied for the synthesis of 2D ZIF layer (ZIF-L) using Hmim: Zn ratio of 8.¹³⁷

5.3. Observation of intermediate phases

Schematic representation of the synthesis procedure of hierarchical porous ZIF-8 is shown in Figure 5.1. PXRD analysis indicates that the white precipitates, formed after the addition of NaOH (0.02-1.0 mmol) to the solution of $\text{Zn}(\text{NO}_3)_2$, are a mixture of the crystalline phase of $\text{Zn}_5(\text{OH})_8(\text{NO}_3)_2 \cdot 2\text{H}_2\text{O}$ (JCPDS card 24-1460) and $\text{Zn}(\text{OH})(\text{NO}_3) \cdot \text{H}_2\text{O}$ (JCPDS card 84-1907) (Figure 5.2). High concentrations of

NaOH (>1.0 mmol) lead to the formation of ZnO nanoparticles (JCPDS card 36-1451, Figure 5.2). SEM images of the formed phases showed that these intermediates arranged as layers ($\text{NaOH} < 1.0$ mmol, Figure 5.3). The phases of $\text{Zn}_5(\text{OH})_8(\text{NO}_3)_2 \cdot 2\text{H}_2\text{O}$, $\text{Zn}(\text{OH})(\text{NO}_3) \cdot \text{H}_2\text{O}$ or ZnO are transformed to pure crystalline ZIF-8 after the addition of Hmim (Figure 5.4).

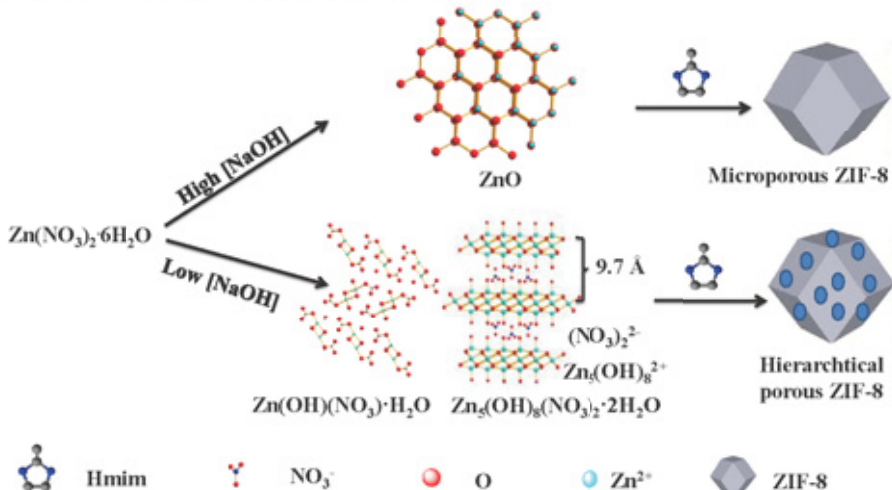


Figure 5.1. Schematic representation for the synthesis of hierarchical porous ZIF-8. Figure reprinted from Paper V.

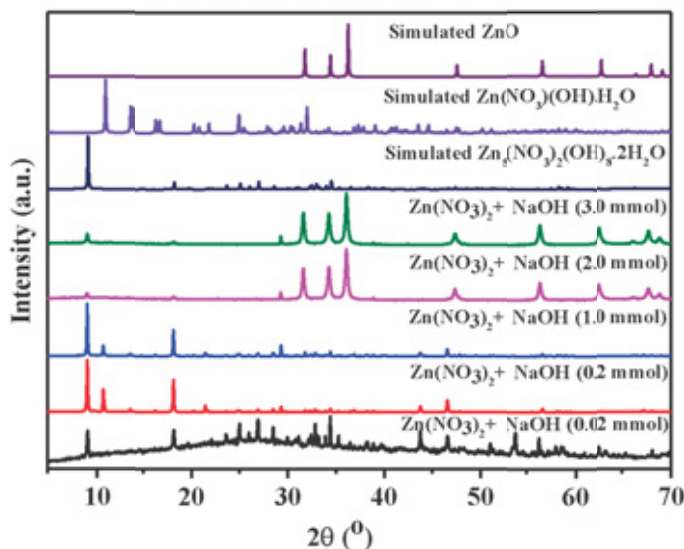


Figure 5.2. PXRD patterns of the intermediates formed after the addition of NaOH (0.02-3.0 mmol) to the solution of $\text{Zn}(\text{NO}_3)_2$. Figure reprinted from Paper V.

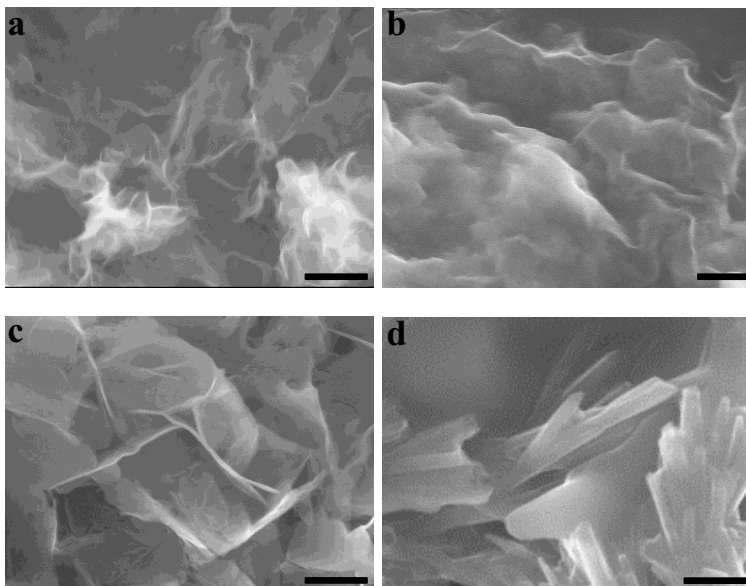


Figure 5.3. SEM images of the phases formed using NaOH of a) 0.02 mmol, b) 0.2 mmol, c) 1.0 mmol, and d) 2 mmol. Scale bars stand for 1 μ m. Figure reprinted from Paper V.

The ratio of Hmim:Zn is critical for the synthesis of the pure phase of ZIF-8 (Figure 5.5)¹³⁸. The synthesis of ZIF-8 in aqueous solution requires high Hmim:Zn (\sim 70)⁷⁴. Figure 5.5 reveals that the optimal molar ratio of our approach is \sim 35. With lower Hmim:Zn ratios \sim 5, 10 and 25, 2D ZIF-L was formed (Figure 5.5). This approach is fast (60 min) and requires low Hmim:Zn ratio (\sim 5) for the synthesis of ZIF-L¹³⁷.

N_2 adsorption isotherms (Figure 5.6) show that low concentrations of NaOH (0.02-0.2 mmol) offer the synthesis of hierarchical porous ZIF-8. High concentrations of NaOH (>1.0 mmol) produce microporous ZIF-8 (Table 5.1). This observation is consistent with the TEM images (Figure 5.7). The particle sizes of ZIF-8 are 50-200 nm (Figure 5.7). The pH values of the reaction mixture increased with the increase of the concentration of NaOH (Figure 5.8). The pH of the reaction mixture is constant over the time after the addition of Hmim (Figure 5.8). The high pH value of the reaction mixture (NaOH $>$ 1 mmol) indicates that the transformation process of ZnO is solid-to-solid transformation¹³⁵. The transformation shows no residual ZnO in the final product ZIF-8¹³⁹.

Table 1 Summary of surface area and pore size using N₂ adsorption-desorption isotherms. Table reprinted from Paper V.

| NaOH (mmol) | Yield (%) | S _{BET} (m ² /g) | S _{Langmuir} (m ² /g) | Pore Vol. a (cm ³ /g) | Micropore Vol. (cm ³ /g) | Meso-pore Vol. (cm ³ /g) |
|-------------|-----------|--------------------------------------|---|-------------------------------------|-------------------------------------|-------------------------------------|
| 0 | 80 | 1597 | 1738 | 0.62 | 0.59 | 0.03 |
| 0.02 | 90 | 1308 | 1332 | 0.59 | 0.42 | 0.17 |
| 0.2 | 90 | 1320 | 1346 | 0.56 | 0.42 | 0.14 |
| 1.0 | 90 | 1552 | 1725 | 0.66 | 0.58 | 0.08 |
| 2.0 | 90 | 1503 | 1641 | 0.59 | 0.55 | 0.04 |
| 3.0 | 91 | 1708 | 1837 | 0.67 | 0.64 | 0.03 |

Note: a, single pore analysis at P/P₀ 0.98; S_{BET}, BET surface area; S_{Langmuir}, Langmuir surface area.

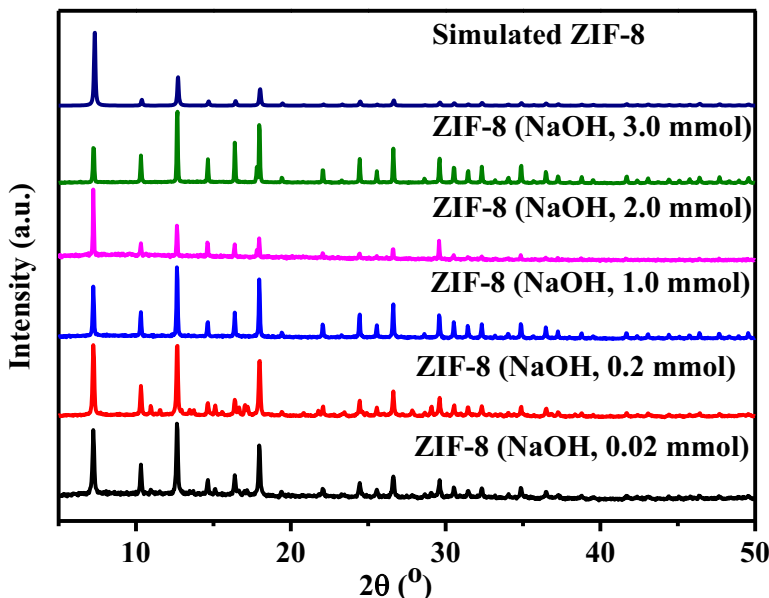


Figure 5.4. PXRD patterns of ZIF-8 using different concentrations of NaOH 0.02-3.0 mmol (Hmim:Zn ratio is 35). Figure reprinted from Paper V.

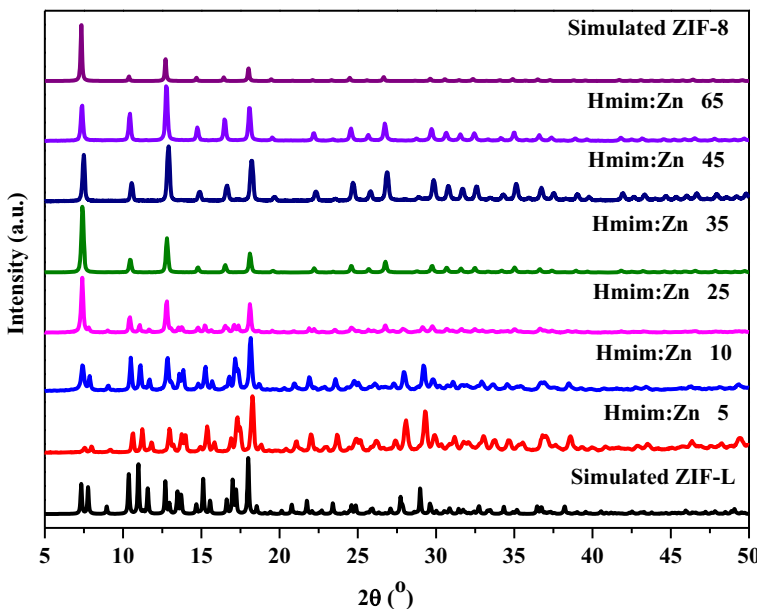


Figure 5.5. PXRD patterns of ZIF-8 using different molar ratios of Hmim:Zn. Figure reprinted from Paper V.

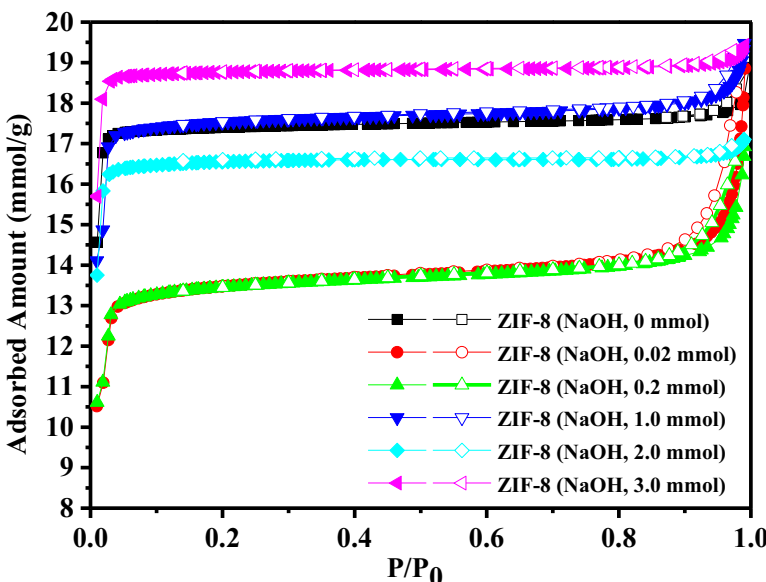


Figure 5.6. N₂ adsorption (closed symbol)-desorption (open symbol) isotherms of ZIF-8 using different concentrations of NaOH (0-3 mmol). Figure reprinted from Paper V.

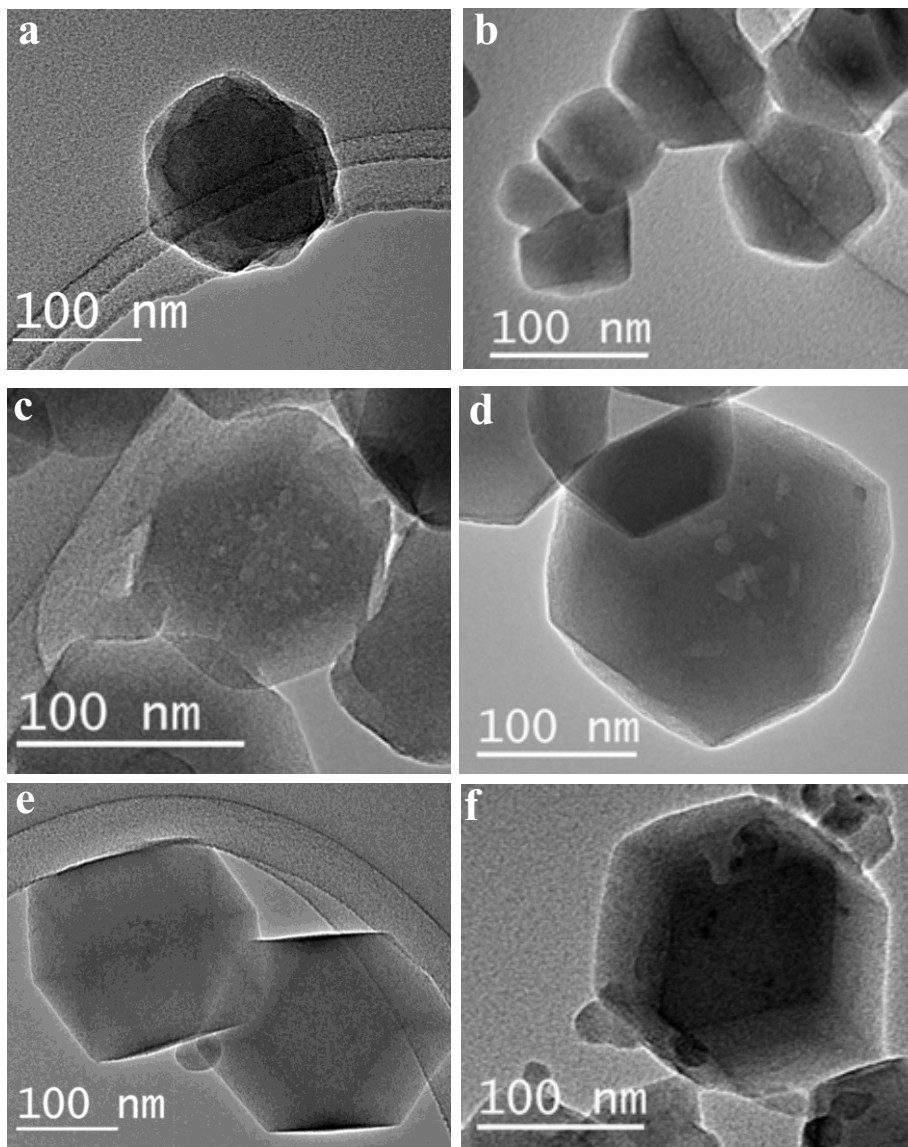


Figure 5.7. TEM images of ZIF-8 synthesized using NaOH; a) 0 mmol, b) 0.02 mmol, c) 0.2 mmol, d) 1.0 mmol, e) 2.0 mmol, and f) 3.0 mmol. Figure reprinted from Paper V.

The current approach is also applied for the synthesis of 2D ZIF-L (Figure 5.9)¹³⁷. TEM images show the leaf morphology of 2D ZIF-L with a broad particle size of 5-12 μm (Figure 2.10).

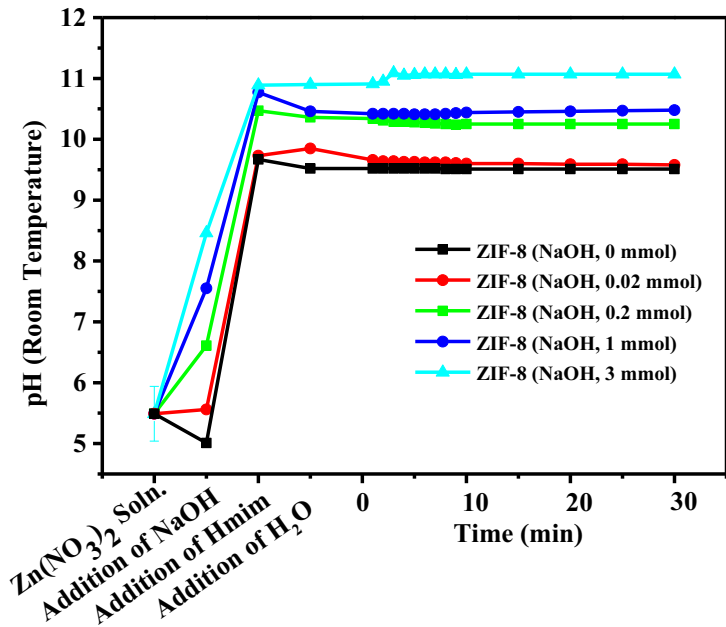


Figure 5.8. pH changes of the reaction mixture during the synthesis of ZIF-8 using NaOH (0-3 mmol). Figure reprinted from Paper V.

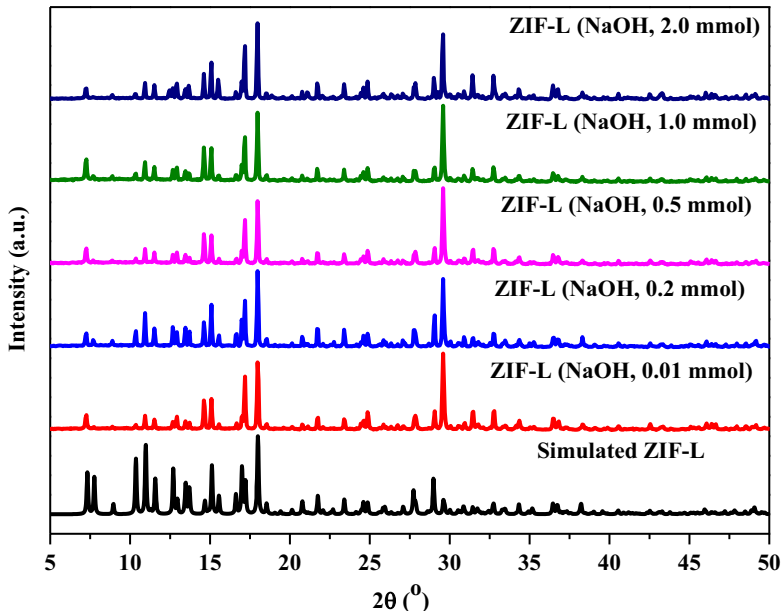


Figure 5.9. PXRD patterns of 2D ZIF-L using NaOH (Hmim:Zn is ~8). Figure reprinted from Paper V.

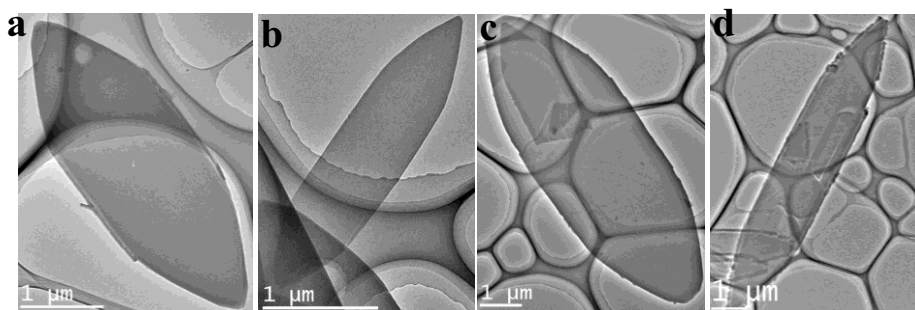


Figure 5.10. TEM images of 2D ZIF-L (Hmim:Zn is ~ 8) using a) 0.01 mmol, b) 0.2 mmol, c) 1 mmol and d) 2 mmol of NaOH. Figure reprinted from Paper V.

5.4. Application of ZIF-8 and ZIF-L for CO₂ sorption

ZIF-8 and ZIF-L show excellent CO₂ adsorption at 298 K (Figure 5.11). Adsorption of CO₂ using ZIF-8 nanoparticles shows the maximum capacity of 0.68-0.86 mmol/g. On the other hand, CO₂ adsorption isotherm of ZIF-L shows maximum adsorption capacity of 0.92-1.02 mmol/g (Figure 5.11). The cushion-shaped cavity of ZIF-L enhances CO₂ sorption compared to ZIF-8 nanoparticles¹³⁷.

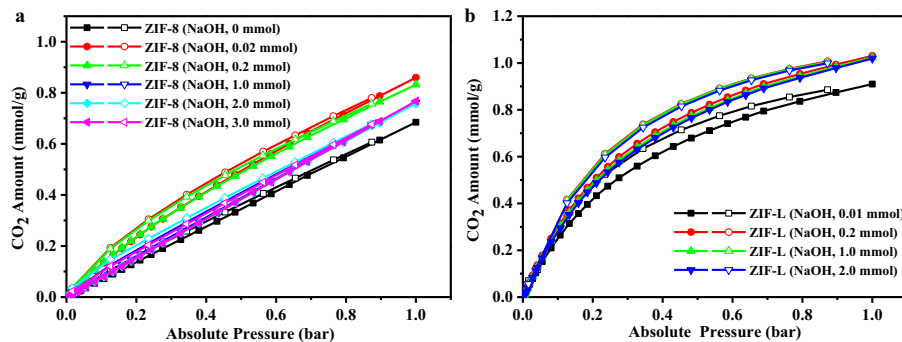


Figure 5.11. CO₂ sorption (298 K) for a) ZIF-8 and b) ZIF-L. Figure reprinted from Paper V.

6. Conclusions

Lanthanide clusters offered highly thermal and chemical stable MOFs. Lanthanide SUMOF-7 (I-IV) series are isoreticular with tunable pore sizes (8.4-23.9 Å) and luminescence properties. Near infrared lanthanide (Pr^{3+} or Nd^{3+}) based SUMOF-7II shows shorter emission lifetimes. The lanthanide MOFs have sharp and narrow emission peak (line-like). The materials have high chemical stability and can be applied for sensing and biosensing. Ferric ions (Fe^{3+}) exhibit selective quenching of the emission signals of SUMOF-7II (La) without a metal chelating agent or other additives. SUMOF-7II show narrower peaks (350-425 nm) and higher emission signals compared to the organic linker. SUMOF-7II (La) offers both qualitative and quantitative analysis of the target metal ion (Fe^{3+}). SUMOF-7II (La) can be applied for selective quantitative analysis of tryptophan among the tested amino acids.

The synthesis of hierarchical porous ZIF-8 using TEA-assisted approach and NaOH is simple and offer tunable porosity. TEA initiates the transformation of zinc nitrate to insoluble ZnO nano rice and lead to the formation of hierarchical porous ZIF-8. The materials contain mesopores of 20-60 nm. This method offers one-pot encapsulation of target species such as dyes and protein. The dye encapsulation provides significant enhancement of the dye's lifetime and may reduce the dye aggregation. The encapsulated dye showed a high tendency to photodegradation under continuous irradiation. The method can also be applied for dye@ZIF-67. However, TEA-assisted approach requires template molecules such as dye or protein. The formation of zinc hydroxide nitrate nanosheets, $\text{Zn}_5(\text{OH})_8(\text{NO}_3)_2 \cdot 2\text{H}_2\text{O}$ and $\text{Zn}(\text{OH})(\text{NO}_3) \cdot \text{H}_2\text{O}$ intermediates, offers *in situ* sacrificial templates for the synthesis of hierarchical porous ZIF-8. The method is template-free and fast. The surface area and the material porosity can be tuned using NaOH. The method has been applied to other ZIFs (2D ZIF-L). ZIF-8 and ZIF-L showed potential application for CO_2 sorption.

7. Future perspectives

This thesis showed few headlines of the synthesis, properties, and applications of stable MOFs. However, there are still many aspects for the future explorations. A few of them are summarized below.

7.1. Study the crystal formation of hierarchical porous ZIF-8

The mechanism of MOF formations is still not understood. The lack of in situ characterization of the crystal formation prevented the full justification of the rationale choice of reaction conditions for the synthetic procedures. To discuss this shortcoming, in situ growth of hierarchical porous ZIF-8 is under investigation using in situ PXRD, fluorescence emission, and FT-IR.

7.2. Multi-variant ZIFs

The synthesis of zeolitic imidazolate frameworks (ZIF-8, ZIF-67, ZIF-L) was reported for one metal node of zinc or cobalt. Multi-variant hierarchical porous ZIFs with more than two tetrahedral metal nodes (Co, Zn, and Cd) have not been explored. Multi-variant ZIFs can be useful for applications such as catalysis.

7.3. Analysis of MOF crystals

Analysis of MOFs usually requires decomposition of the material before the analysis. This method not only is destructive, but also could lead to misconception. A further analytical protocol such as mass spectrometry should be carried out. The large surface area of MOFs may provide a surface for surface enhanced laser desorption/ionization mass spectrometry, and thus facilitate the analysis^{140,141}.

7.4. Applications of dye@ZIF-8

Dye encapsulated ZIF-8 is promising for several applications including sensing, biosensing, solar cells applications, and others. The dye encapsulated ZIF-8 could be a useful probe for sensing and biosensing applications of many analytes such as adenosine triphosphate¹⁴². I synthesized solar cell dye encapsulated ZIF-8 and further investigations are undergoing.

8. Acknowledgements

I would like to thank my supervisor, Prof. Xiaodong Zou, for her advice and support during my doctoral studies. Many thanks for giving me the freedom to select my own direction, and for sharing her knowledge, and time.

I would like to thank my co-supervisor, Prof. Belén Martín-Matute, for offering me the organic linkers. Many thanks to the funding agencies, the Swedish Research Council (VR), the Swedish Governmental Agency for Innovation Systems (VINNOVA), and the Röntgen-Ångström Cluster. Thanks to Berzelii Center EXSELENT for travel grant.

Thanks to my collaborators: Dr. A. Bermejo Gómez, Dr. A. El-Zohry, Dr. H. Zheng, Dr. Z. Huang, Dr. J. Su, Dr. W. Wan, Dr. Y. Yun, Dr. V. Pascanu, A. S. Etman, Dr. Q. Yao, Alejandro, Dr. T. Thersleff, M. Naeem and Prof. A.-V. Mudring, Dr. M. Wilk, Dr. R. Ashour, Dr. A. Abdel-Magied, Prof. A. Abdelkhalek, Prof. M. Ali, A. Uheida, Prof. M. Muhammed, Prof. J. Dutta, Dr. M. Dowaidar, Dr. M. Hällbrink, Dr. K. Kurrikoff, K. Freimann, Prof. Ü. Langel, Dr. K. Hussein, Prof. H.M. Woo, Prof. J. Sun, P. Rzepka, A. Shatskiy, Prof. B. Åkermark, M. Kärkäs, and Dr. E. Johnston.

Thanks to everybody, past and present members, in Xiaodong's and Belén's groups: Dr. F. Carson, Dr. A. Platero-Prats, Dr. T. Willhammar, Dr. H. Chen, Dr. I. Ibarra, Dr. P. Guo, Dr. A.K. Inge, L.Yunxiang, E. Kapaca, Y.Zheng, F. Peng, J. Liang, N. Yuan, Qingping, Dr. H.Xu, M. Cichocka, J. Lin, Dr. F. Gao, T. Yang, B. Wang, Dr. S. Smeets and Dr. Liu. Thanks to the colleagues of MMK; I. Ermilova, D.O. Ojwang, A. Neagu, M. Chamoun, D. Eklöf, L.A. Valencia Lopez, Y. Trushkina, K. Gordeyeva, V. Guccini, T. Church, and other. Thanks to colleagues from other departments; H.Moubarak (Ogranic), A. Ramzy (ACES), H. Elmongy (ACES), Dr. K. Ezzat (KI).

Thanks to all the lecturers, professors, guest teachers and staff at MMK for sharing your knowledge, notes, and lectures: Prof. L. Bergström, Prof. N. Hedin, Prof. M. Johnsson, Prof. J. Grins, Prof. L. Eriksson, Prof. O. Terasaki, Prof. K. Jansson, Dr. Z. Bacsik, Prof. S. Hovmöller, Prof. U. Häussermann, Prof. J. Kowalewski, Prof. A. Maliniak, Prof. L. McCusker, Prof. G. Salazar Alvarez, Prof. J. Z. Shen, Dr. A. Ertan and Dr. C.-W. Tai.

Thank you to those working in the administration offices for your constant help: A.-B. Rönnell, C. Berg, D. Emanuelsson, T. Bulavina,

A. Loftsjö, H. Frejman, P. Raninen, and R. Eriksson. Thanks for the workshop staffs for your kind help.

Thanks to the Ministry of Higher Education and Assuit University (Egypt) for support during my studies. I would like to thank my professors; Prof. A.A. Geies (President of Assiut University), Prof. K. Ibrahim (head of department), Prof. E. Zinati, Prof. T. El-Gammal, Prof. M. Abdullahtif Jadel-Mola, Prof. H. El-Hawary, Prof. A. Abushaly, Prof. N. Abo Elmaali, Prof. Sadek, Prof. Khalaf, Prof. Ibrahim, Prof. Hammam, Prof. Edrees, Prof. Ali, Prof. El-kashef, Prof. El-sheref, Prof. Youssef, Prof. Abdel-aal Hasan, Prof. Abdel-rahman, Prof. Abdel Wahhab, Prof. Hussien, Prof. Ibrahim, Prof. Tmirk, Prof. Aref, Prof. Saleh, Prof. Mostafa, Prof. Ibrahim, Prof. Harb, Prof. Abdel-galeel, Prof. Said, Prof. Mohamed, Prof. Abd allah, Prof. Gomaa, Prof. Girgis, Prof. Abdel-rahman, Prof. Saber, Prof. Abdel-wahab, Prof. Abdel-Aal, Prof. Sedira, Prof. Mohseb, Prof. El-Awad, Prof. Ali, Prof. Bakheet, Prof. Ibrahim, Prof. Ghandoor, Prof. Abdullah EL-Gahami, Prof. Mahmoud, Prof. Hasan, Prof. Hashem, Prof. Amara, Prof. Khalil, Prof. Ibrahim, Prof. Ellethy, Prof. Abdallah Hermas, Prof. Mahmoud, Prof. Abu-Zied, Prof. Saleh, Prof. Farag, Prof. Abdel-Wahab, Prof. Ahmed, Prof. Mohamed, Prof. El-Emary, Prof. Farghaly, Prof. A. Mostafa, Prof. Hasanian, Prof. Abdel-Moneim, Prof. Mostafa, Dr. Ebraheem, Dr. A.El-moniem, Dr. Khafaji, Dr. Wahdan, Dr. Othman, Dr. Ahmed, Dr. Sayed, Dr. Ali, Dr. Fahmy, Dr. Ali, Dr. Farrage, Dr. Sayed, Dr. Abd El-Aal, Dr. Yusef, Dr. Abdel-SAbor, Dr. Farghaly, Dr. Aly, Dr. Youssef, Dr. Abdel-Rahman, Dr. Zaki Asal, Dr. Ahmed, Dr. Ibrahim, Dr. Farrag, Dr. Ahmed, Dr. Ibrahim, Dr. Abdel-baky, Dr. Said, Dr. Abdel-Hafez, Dr. Nada, Saied, Dr. Nady, Mansoure, Mohamed, Soliman, Osman, AbdEl-Aal, Saddik, Dr. Abdel-megeed , Dr. Qasim, Mohamed, D. Abdel-kader, Gamal Eldin, A. Hassan, M. Kamal,O. Nasr, M. Mohamed, M. Abdelshakour, A. Fathy, A. Abotaleb, H. Eldeen Atteia, M. Mahmoud, R. Mamdoh, L. Sabry, M. Osama, Abo Markeb, Eshaaq, Mohamed, Fouad. Thanks to Prof. M. El-shazly (Ain Shams University) for his help.

Thanks to all my friends and colleagues who supported me physically, mentally, and emotionally during these four years (2013-2017).

I would express my all gratitude to my parents, wife, sisters, and brother. There would have been no thesis without the support of my family.

9. References

- (1) Rouquerol, F.; Rouquerol, J.; Sing, K. S. W.; Llewellyn, P.; Maurin, G. In *Climate Change 2013 - The Physical Science Basis*; Intergovernmental Panel on Climate Change, Ed.; Cambridge University Press: Cambridge, 2014; pp 1–30.
- (2) Slater, A. G.; Cooper, A. I. *Science*. **2015**, *348* (6238), aaa8075–aaa8075.
- (3) Yaghi, O. M.; Li, H. *J. Am. Chem. Soc.* **1995**, *117* (41), 10401–10402.
- (4) Tranchemontagne, D. J.; Mendoza-Cortés, J. L.; O’Keeffe, M.; Yaghi, O. M. *Chem. Soc. Rev.* **2009**, *38* (5), 1257.
- (5) Li, H.; Eddaoudi, M.; Groy, T. L.; Yaghi, O. M. *J. Am. Chem. Soc.* **1998**, *120* (33), 8571–8572.
- (6) Furukawa, H.; Ko, N.; Go, Y. B.; Aratani, N.; Choi, S. B.; Choi, E.; Yazaydin, A. O.; Snurr, R. Q.; O’Keeffe, M.; Kim, J.; Yaghi, O. M. *Science*. **2010**, *329* (5990), 424–428.
- (7) Ma, L.; Abney, C.; Lin, W. *Chem. Soc. Rev.* **2009**, *38* (5), 1248.
- (8) Zhu, Q.-L.; Xu, Q. *Chem. Soc. Rev.* **2014**, *43* (16), 5468–5512.
- (9) Cohen, S. M. *Chem. Rev.* **2012**, *112* (2), 970–1000.
- (10) Dhakshinamoorthy, A.; Garcia, H. *Chem. Soc. Rev.* **2012**, *41* (15), 5262.
- (11) Czaja, A. U.; Trukhan, N.; Müller, U. *Chem. Soc. Rev.* **2009**, *38* (5), 1284.
- (12) Lee, J.; Farha, O. K.; Roberts, J.; Scheidt, K. A.; Nguyen, S. T.; Hupp, J. T. *Chem. Soc. Rev.* **2009**, *38* (5), 1450.
- (13) Farrusseng, D.; Aguado, S.; Pinel, C. *Angew. Chemie Int. Ed.* **2009**, *48* (41), 7502–7513.
- (14) Férey, G. *Chem. Soc. Rev.* **2008**, *37* (1), 191–214.
- (15) Li, M.; Li, D.; O’Keeffe, M.; Yaghi, O. M. *Chem. Rev.* **2014**, *114* (2), 1343–1370.
- (16) First, E. L.; Floudas, C. A. *Microporous Mesoporous Mater.* **2013**, *165*, 32–39.
- (17) Moghadam, P. Z.; Li, A.; Wiggin, S. B.; Tao, A.; Maloney, A. G. P.; Wood, P. A.; Ward, S. C.; Fairen-Jimenez, D. *Chem. Mater.* **2017**, *29* (7), 2618–2625.
- (18) Furukawa, H.; Cordova, K. E.; O’Keeffe, M.; Yaghi, O. M. *Science (80-.).* **2013**, *341* (6149), 1230444–1230444.
- (19) Kauffman, G. B. *Alfred Werner*; Springer Berlin Heidelberg: Berlin, Heidelberg, 1966.
- (20) Hofmann, K. A.; Küspert, F. *Zeitschrift für Anorg. Chemie*

- 1897**, 15 (1), 204–207.
- (21) Rayner, J. H.; Powell, H. M. *J. Chem. Soc.* **1952**, 0 (0), 319–328.
- (22) He, Y.; Li, B.; O’Keeffe, M.; Chen, B. *Chem. Soc. Rev.* **2014**, 43 (16), 5618–5656.
- (23) Brozek, C. K.; Dincă, M. *Chem. Soc. Rev.* **2014**, 43 (16), 5456–5467.
- (24) Evans, J. D.; Sumby, C. J.; Doonan, C. J. *Chem. Soc. Rev.* **2014**, 43 (16), 5933–5951.
- (25) Koh, K.; Wong-Foy, A. G.; Matzger, A. J. *Angew. Chemie Int. Ed.* **2008**, 47 (4), 677–680.
- (26) Zhang, B.; Zhang, J.; Liu, C.; Sang, X.; Peng, L.; Ma, X.; Wu, T.; Han, B.; Yang, G. *RSC Adv.* **2015**, 5 (47), 37691–37696.
- (27) Yue, Y.; Qiao, Z.-A.; Fulvio, P. F.; Binder, A. J.; Tian, C.; Chen, J.; Nelson, K. M.; Zhu, X.; Dai, S. *J. Am. Chem. Soc.* **2013**, 135 (26), 9572–9575.
- (28) Xue, Z.; Zhang, J.; Peng, L.; Han, B.; Mu, T.; Li, J.; Yang, G. *ChemPhysChem* **2014**, 15 (1), 85–89.
- (29) Guo, H.; Zhu, Y.; Wang, S.; Su, S.; Zhou, L.; Zhang, H. *Chem. Mater.* **2012**, 24 (3), 444–450.
- (30) Tsuruoka, T.; Furukawa, S.; Takashima, Y.; Yoshida, K.; Isoda, S.; Kitagawa, S. *Angew. Chemie Int. Ed.* **2009**, 48 (26), 4739–4743.
- (31) Stock, N.; Biswas, S. *Chem. Rev.* **2012**, 112 (2), 933–969.
- (32) Ahmad, N.; Younus, H. A.; Chughtai, A. H.; Verpoort, F. *Chem. Soc. Rev.* **2015**, 44 (1), 9–25.
- (33) Falcaro, P.; Ricco, R.; Doherty, C. M.; Liang, K.; Hill, A. J.; Styles, M. J. *Chem. Soc. Rev.* **2014**, 43 (16), 5513–5560.
- (34) Janiak, C.; Vieth, J. K. *New J. Chem.* **2010**, 34 (11), 2366.
- (35) Wang, S.; Wang, X. *Small* **2015**, 11 (26), 3097–3112.
- (36) Cui, Y.; Chen, B.; Qian, G. *Coord. Chem. Rev.* **2014**, 273–274, 76–86.
- (37) Ke, F.-S.; Wu, Y.-S.; Deng, H. *J. Solid State Chem.* **2015**, 223, 109–121.
- (38) Low, J. J.; Benin, A. I.; Jakubczak, P.; Abrahamian, J. F.; Faheem, S. A.; Willis, R. R. *J. Am. Chem. Soc.* **2009**, 131 (43), 15834–15842.
- (39) Zhang, W.; Hu, Y.; Ge, J.; Jiang, H.-L.; Yu, S.-H. *J. Am. Chem. Soc.* **2014**, 136 (49), 16978–16981.
- (40) Bradshaw, D.; El-Hankari, S.; Lupica-Spagnolo, L. *Chem. Soc. Rev.* **2014**, 43 (16), 5431–5443.

- (41) Eddaoudi, M.; Kim, J.; Rosi, N.; Vodak, D.; Wachter, J.; O'Keeffe, M.; Yaghi, O. M. *Science* **2002**, *295* (5554), 469–472.
- (42) Yao, Q.; Bermejo Gómez, A.; Su, J.; Pascanu, V.; Yun, Y.; Zheng, H.; Chen, H.; Liu, L.; Abdelhamid, H. N.; Martín-Matute, B.; Zou, X. *Chem. Mater.* **2015**, *27* (15), 5332–5339.
- (43) Feng, D.; Wang, K.; Su, J.; Liu, T. F.; Park, J.; Wei, Z.; Bosch, M.; Yakovenko, A.; Zou, X.; Zhou, H. C. *Angew. Chemie - Int. Ed.* **2015**, *54* (1), 149–154.
- (44) Zou, X.; Yao, Q.; Gómez, A. B.; Su, J.; Pascanu, V.; Yun, Y.; Zheng, H.; Chen, H.; Liu, L.; Abdelhamid, H. N.; Martín-Matute, B. *Acta Crystallogr. Sect. A Found. Adv.* **2016**, *72* (a1), s136–s136.
- (45) Peng, L.; Zhang, J.; Xue, Z.; Han, B.; Sang, X.; Liu, C.; Yang, G. *Nat. Commun.* **2014**, *5*, 933–969.
- (46) Zheng, H.; Zhang, Y.; Liu, L.; Wan, W.; Guo, P.; Nyström, A. M.; Zou, X. *J. Am. Chem. Soc.* **2016**, *138* (3), 962–968.
- (47) He, S.; Chen, Y.; Zhang, Z.; Ni, B.; He, W.; Wang, X. *Chem. Sci.* **2016**, *7* (12), 7101–7105.
- (48) Zheng, H.; Zhang, Y.; Liu, L.; Wan, W.; Guo, P.; Nyström, A. M.; Zou, X. *J. Am. Chem. Soc.* **2016**, *138* (3), 962–968.
- (49) *Lanthanide Metal-Organic Frameworks*; Cheng, P., Ed.; Structure and Bonding; Springer Berlin Heidelberg: Berlin, Heidelberg, 2015; Vol. 163.
- (50) Xu, L.-J.; Xu, G.-T.; Chen, Z.-N. *Coord. Chem. Rev.* **2014**, *273–274*, 47–62.
- (51) Hu, Z.; Deibert, B. J.; Li, J. *Chem. Soc. Rev.* **2014**, *43* (16), 5815–5840.
- (52) An, J.; Shade, C. M.; Chengelis-Czegan, D. A.; Petoud, S.; Rosi, N. L. *J. Am. Chem. Soc.* **2011**, *133* (5), 1220–1223.
- (53) Cho, W.; Lee, H. J.; Choi, G.; Choi, S.; Oh, M. *J. Am. Chem. Soc.* **2014**, *136* (35), 12201–12204.
- (54) Zhang, X.; Wang, W.; Hu, Z.; Wang, G.; Uvdal, K. *Coord. Chem. Rev.* **2015**, *284*, 206–235.
- (55) Müller-Buschbaum, K.; Beuerle, F.; Feldmann, C. *Microporous Mesoporous Mater.* **2015**, *216*, 171–199.
- (56) Rocha, J.; Carlos, L. D.; Paz, F. A. A.; Ananias, D. *Chem. Soc. Rev.* **2011**, *40* (2), 926–940.
- (57) Bünzli, J.-C. G.; Eliseeva, S. V. In *Comprehensive Inorganic Chemistry II*; Elsevier, 2013; pp 339–398.
- (58) Kreno, L. E.; Leong, K.; Farha, O. K.; Allendorf, M.; Van

- Duyne, R. P.; Hupp, J. T. *Chem. Rev.* **2012**, *112* (2), 1105–1125.
- (59) Yang, Y.; Shen, K.; Lin, J.; Zhou, Y.; Liu, Q.; Hang, C.; Abdelhamid, H. N.; Zhang, Z.; Chen, H. *RSC Adv.* **2016**, *6* (51), 45475–45481.
- (60) Lin, R.-B.; Liu, S.-Y.; Ye, J.-W.; Li, X.-Y.; Zhang, J.-P. *Adv. Sci.* **2016**, *3* (7), 1500434.
- (61) Lu, G.; Hupp, J. T. *J. Am. Chem. Soc.* **2010**, *132* (23), 7832–7833.
- (62) Wang, R.; Liu, X.; Huang, A.; Wang, W.; Xiao, Z.; Zhang, L.; Dai, F.; Sun, D. *Inorg. Chem.* **2016**, *55* (4), 1782–1787.
- (63) Chen, Y.-Z.; Jiang, H.-L. *Chem. Mater.* **2016**, *28* (18), 6698–6704.
- (64) Abdelhamid, H. N. *TrAC Trends Anal. Chem.* **2017**, *89*, 68–98.
- (65) Park, K. S.; Ni, Z.; Cote, A. P.; Choi, J. Y.; Huang, R.; Uribe-Romo, F. J.; Chae, H. K.; O’Keeffe, M.; Yaghi, O. M. *Proc. Natl. Acad. Sci.* **2006**, *103* (27), 10186–10191.
- (66) Chen, B.; Yang, Z.; Zhu, Y.; Xia, Y. *J. Mater. Chem. A* **2014**, *2* (40), 16811–16831.
- (67) Zhou, K.; Mousavi, B.; Luo, Z.; Phatanasri, S.; Chaemchuen, S.; Verpoort, F. *J. Mater. Chem. A* **2017**, *5* (3), 952–957.
- (68) Stassen, I.; Styles, M.; Grenci, G.; Gorp, H. Van; Vanderlinden, W.; Feyter, S. De; Falcaro, P.; Vos, D. De; Vereecken, P.; Ameloot, R. *Nat. Mater.* **2015**, *15*, 304–310.
- (69) Yamamoto, D.; Maki, T.; Watanabe, S.; Tanaka, H.; Miyahara, M. T.; Mae, K. *Chem. Eng. J.* **2013**, *227*, 145–150.
- (70) Yang, L.; Lu, H. *Chinese J. Chem.* **2012**, *30* (5), 1040–1044.
- (71) Shi, Q.; Chen, Z.; Song, Z.; Li, J.; Dong, J. *Angew. Chem. Int. Ed. Engl.* **2011**, *50* (3), 672–675.
- (72) Beldon, P. J.; Fábián, L.; Stein, R. S.; Thirumurugan, A.; Cheetham, A. K.; Friščić, T. *Angew. Chem. Int. Ed. Engl.* **2010**, *49* (50), 9640–9643.
- (73) Seoane, B.; Zamaro, J. M.; Tellez, C.; Coronas, J. *CrystEngComm* **2012**, *14* (9), 3103.
- (74) Pan, Y.; Liu, Y.; Zeng, G.; Zhao, L.; Lai, Z. *Chem. Commun.* **2011**, *47* (7), 2071–2073.
- (75) Chizallet, C.; Lazare, S.; Bazer-Bachi, D.; Bonnier, F.; Lecocq, V.; Soyer, E.; Quoineaud, A.-A.; Bats, N. *J. Am. Chem. Soc.* **2010**, *132* (35), 12365–12377.
- (76) Tran, U. P. N.; Le, K. K. A.; Phan, N. T. S. *ACS Catal.* **2011**, *1* (2), 120–127.

- (77) Kalidindi, S. B.; Esken, D.; Fischer, R. A. *Chem. - A Eur. J.* **2011**, *17* (24), 6594–6597.
- (78) McEwen, J.; Hayman, J.-D.; Ozgur Yazaydin, A. *Chem. Phys.* **2013**, *412*, 72–76.
- (79) Gee, J. A.; Chung, J.; Nair, S.; Sholl, D. S. *J. Phys. Chem. C* **2013**, *117* (6), 3169–3176.
- (80) Mosier, A. M.; Larson, H. L. W.; Webster, E. R.; Ivos, M.; Tian, F.; Benz, L. *Langmuir* **2016**, *32* (12), 2947–2954.
- (81) Jiang, J.-Q.; Yang, C.-X.; Yan, X.-P. *ACS Appl. Mater. Interfaces* **2013**, *5* (19), 9837–9842.
- (82) Wu, Y.; Zhou, M.; Zhang, B.; Wu, B.; Li, J.; Qiao, J.; Guan, X.; Li, F. *Nanoscale* **2014**, *6* (2), 1105–1112.
- (83) Zheng, H.; Zhang, Y.; Liu, L.; Wan, W.; Guo, P.; Nyström, A. M.; Zou, X. **2016**.
- (84) Stassen, I.; Styles, M.; Grenci, G.; Gorp, H. V.; Vanderlinden, W.; Feyter, S. D.; Falcaro, P.; Vos, D. De; Vereecken, P.; Ameloot, R. *Nat. Mater.* **2015**, *15* (3), 304–310.
- (85) Stavila, V.; Talin, A. A.; Allendorf, M. D. *Chem. Soc. Rev.* **2014**, *43* (16), 5994–6010.
- (86) Qiu, S.; Xue, M.; Zhu, G. *Chem. Soc. Rev.* **2014**, *43* (16), 6116–6140.
- (87) Sumida, K.; Rogow, D. L.; Mason, J. A.; McDonald, T. M.; Bloch, E. D.; Herm, Z. R.; Bae, T.-H.; Long, J. R. *Chem. Rev.* **2012**, *112* (2), 724–781.
- (88) Nugent, P.; Belmabkhout, Y.; Burd, S. D.; Cairns, A. J.; Luebke, R.; Forrest, K.; Pham, T.; Ma, S. Q.; Space, B.; Wojtas, L.; Eddaoudi, M.; Zaworotko, M. J. *Nature* **2013**, *495* (7439), 80–84.
- (89) Liu, J.; Thallapally, P. K.; McGrail, B. P.; Brown, D. R.; Liu, J. *Chem. Soc. Rev.* **2012**, *41* (6), 2308–2322.
- (90) Caskey, S. R.; Wong-Foy, A. G.; Matzger, A. J. *J. Am. Chem. Soc.* **2008**, *130* (33), 10870–10871.
- (91) Munn, A. S.; Dunne, P. W.; Tang, S. V. Y.; Lester, E. H. *Chem. Commun.* **2015**, *51* (64), 12811–12814.
- (92) Yao, Q.; Su, J.; Zou, X. *Zeitschrift für Krist. - Cryst. Mater.* **2013**, *228* (7), 323–329.
- (93) Harris, K. D. M.; Tremayne, M.; Kariuki, B. M. *Angew. Chemie Int. Ed.* **2001**, *40* (9), 1626–1651.
- (94) Abdelhamid, H. N.; Bermejo-Gómez, A.; Martín-Matute, B.; Zou, X. *Microchim. Acta* **2017**, *184* (9), 3363–3371.
- (95) Abdelhamid, H. N.; Huang, Z.; El-Zohry, A. M.; Zheng, H.;

- Zou, X. *Inorg. Chem.* **2017**, *56* (15), 9139–9146.
- (96) Grant Bunker. *Introduction to XAFS: A Practical Guide to X-ray Absorption Fine Structure Spectroscopy*; Cambridge University Press, 2010.
- (97) Jalilehvand, F. Structure of hydrated ions and cyano complexes by x-absorption spectroscopy, KTH Royal Institute of Technology, 2000.
- (98) Erni, R.; Rossell, M. D.; Kisielowski, C.; Dahmen, U. *Phys. Rev. Lett.* **2009**, *102* (9), 96101.
- (99) Williams, D. B.; Carter, C. B. *Transmission Electron Microscopy*; Springer US: Boston, MA, 2009.
- (100) Zou, X.; Hovmöller, S.; Oleynikov, P. *Electron CrystallographyElectron Microscopy and Electron Diffraction*; Oxford University Press, 2011.
- (101) Rouquerol, J. *Characterization of porous solids III: proceedings of the IUPAC symposium (COPS III), Marseille, France ... 1993*; Elsevier, 1994; Vol. 87.
- (102) Emmett, P. H.; Brunauer, S. *J. Am. Chem. Soc.* **1937**, *59* (8), 1553–1564.
- (103) A. D. McNaught and A. Wilkinson. Blackwell Scientific Publications, O. *IUPAC Compendium of Chemical Terminology*; Nič, M., Jirát, J., Košata, B., Jenkins, A., McNaught, A., Eds.; IUPAC: Research Triangle Park, NC, 2009.
- (104) Sing, K. S. W. *Pure Appl. Chem.* **1985**, *57* (4), 603–619.
- (105) Furukawa, H.; Ko, N.; Go, Y. B.; Aratani, N.; Choi, S. B.; Choi, E.; Yazaydin, A. O.; Snurr, R. Q.; O’Keeffe, M.; Kim, J.; Yaghi, O. M. *Science*. **2010**, *329* (5990), 424–428.
- (106) Lakowicz, J. R. *Principles of Fluorescence Spectroscopy*; Lakowicz, J. R., Ed.; Springer US: Boston, MA, 2006.
- (107) Guo, X.; Zhu, G.; Li, Z.; Sun, F.; Yang, Z.; Qiu, S. *Chem. Commun.* **2006**, *0* (30), 3172–3174.
- (108) Gustafsson, M.; Bartoszewicz, A.; Martín-Matute, B.; Sun, J.; Grins, J.; Zhao, T.; Li, Z.; Zhu, G.; Zou, X. *Chem. Mater.* **2010**, *22* (11), 3316–3322.
- (109) Tan, K.; Nijem, N.; Canepa, P.; Gong, Q.; Li, J.; Thonhauser, T.; Chabal, Y. J. *J. Chem. Mater.* **2012**, *24* (16), 3153–3167.
- (110) Carlos, L. D.; Ferreira, R. A. S.; de Zea Bermudez, V.; Julián-López, B.; Escribano, P. *Chem. Soc. Rev.* **2011**, *40* (2), 536–549.
- (111) Bünzli, J.-C. G.; Eliseeva, S. V. *Comprehensive Inorganic Chemistry II*; Elsevier, 2013.

- (112) Cui, Y.; Yue, Y.; Qian, G.; Chen, B. *Chem. Rev.* **2012**, *112* (2), 1126–1162.
- (113) Zhang, H.-J.; Wang, X.-Z.; Zhu, D.-R.; Song, Y.; Xu, Y.; Xu, H.; Shen, X.; Gao, T.; Huang, M.-X. *CrystEngComm* **2011**, *13* (7), 2586.
- (114) Berezin, M. Y.; Achilefu, S. *Chem. Rev.* **2010**, *110* (5), 2641–2684.
- (115) Devic, T.; Wagner, V.; Guillou, N.; Vimont, A.; Haouas, M.; Pascolini, M.; Serre, C.; Marrot, J.; Daturi, M.; Taulelle, F.; Férey, G. *Microporous Mesoporous Mater.* **2011**, *140* (1–3), 25–33.
- (116) Ananias, D.; Brites, C. D. S.; Carlos, L. D.; Rocha, J. *Eur. J. Inorg. Chem.* **2016**, *2016* (13–14), 1967–1971.
- (117) Zheng, M.; Tan, H.; Xie, Z.; Zhang, L.; Jing, X.; Sun, Z. *ACS Appl. Mater. Interfaces* **2013**, *5* (3), 1078–1083.
- (118) Yang, C.-X.; Ren, H.-B.; Yan, X.-P. *Anal. Chem.* **2013**, *85* (15), 7441–7446.
- (119) Park, K. S.; Ni, Z.; Cote, A. P.; Choi, J. Y.; Huang, R.; Uribe-Romo, F. J.; Chae, H. K.; O’Keeffe, M.; Yaghi, O. M. *Proc. Natl. Acad. Sci. U. S. A.* **2006**, *103* (27), 10186–10191.
- (120) Banerjee, R.; Phan, A.; Wang, B.; Knobler, C.; Furukawa, H.; O’Keeffe, M.; Yaghi, O. M. *Science* **2008**, *319* (5865), 939–943.
- (121) Cacho-Bailo, F.; Seoane, B.; Téllez, C.; Coronas, J. *J. Memb. Sci.* **2014**, *464*, 119–126.
- (122) Yurderi, M.; Bulut, A.; Zahmakiran, M.; Gülcen, M.; Özkar, S. *Appl. Catal. B Environ.* **2014**, *160*–*161*, 534–541.
- (123) Wang, Z.; Dou, Z.; Cui, Y.; Yang, Y.; Wang, Z.; Qian, G. *Microporous Mesoporous Mater.* **2014**, *185*, 92–96.
- (124) Park, K. S.; Ni, Z.; Côté, A. P.; Choi, J. Y.; Huang, R.; Uribe-Romo, F. J.; Chae, H. K.; O’Keeffe, M.; Yaghi, O. M. *Proc. Natl. Acad. Sci. U. S. A.* **2006**, *103* (27), 10186–10191.
- (125) Wang, S.; Fan, Y.; Jia, X. *Chem. Eng. J.* **2014**, *256*, 14–22.
- (126) Cao, S.; Gody, G.; Zhao, W.; Perrier, S.; Peng, X.; Ducati, C.; Zhao, D.; Cheetham, A. K. *Chem. Sci.* **2013**, *4* (9), 3573.
- (127) Wu, Y.; Zhou, M.; Zhang, B.; Wu, B.; Li, J.; Qiao, J.; Guan, X.; Li, F. *Nanoscale* **2014**, *6* (2), 1105–1112.
- (128) Jian, M.; Liu, B.; Zhang, G.; Liu, R.; Zhang, X. *Colloids Surfaces A Physicochem. Eng. Asp.* **2015**, *465*, 67–76.
- (129) He, M.; Yao, J.; Liu, Q.; Wang, K.; Chen, F.; Wang, H. *Microporous Mesoporous Mater.* **2014**, *184*, 55–60.

- (130) Low, Z.-X.; Yao, J.; Liu, Q.; He, M.; Wang, Z.; Suresh, A. K.; Bellare, J.; Wang, H. *Cryst. Growth Des.* **2014**, *14* (12), 6589–6598.
- (131) Ahmed, A.; Forster, M.; Jin, J.; Myers, P.; Zhang, H. *ACS Appl. Mater. Interfaces* **2015**, *7* (32), 18054–18063.
- (132) Wu, X.; Ge, J.; Yang, C.; Hou, M.; Liu, Z. *Chem. Commun.* **2015**, *51* (69), 13408–13411.
- (133) Wu, Y.; Zhou, M.; Zhang, B.; Wu, B.; Li, J.; Qiao, J.; Guan, X.; Li, F. *Nanoscale* **2014**, *6* (2), 1105–1112.
- (134) Cao, S.; Gody, G.; Zhao, W.; Perrier, S.; Peng, X.; Ducati, C.; Zhao, D.; Cheetham, A. K. *Chem. Sci.* **2013**, *4* (9), 3573–3577.
- (135) Stassen, I.; Styles, M.; Grenci, G.; Gorp, H. V.; Vanderlinden, W.; Feyter, S. D.; Falcaro, P.; Vos, D. De; Vereecken, P.; Ameloot, R. *Nat. Mater.* **2015**, *15* (3), 304–310.
- (136) Katsenis, A. D.; Puškarić, A.; Štrukil, V.; Mottillo, C.; Julien, P. A.; Užarević, K.; Pham, M.-H.; Do, T.-O.; Kimber, S. A. J.; Lazić, P.; Magdysyuk, O.; Dinnebier, R. E.; Halasz, I.; Friščić, T. *Nat. Commun.* **2015**, *6*, 6662.
- (137) Chen, R.; Yao, J.; Gu, Q.; Smeets, S.; Baerlocher, C.; Gu, H.; Zhu, D.; Morris, W.; Yaghi, O. M.; Wang, H. *Chem. Commun.* **2013**, *49* (82), 9500–9502.
- (138) Kida, K.; Okita, M.; Fujita, K.; Tanaka, S.; Miyake, Y. *CrystEngComm* **2013**, *15* (9), 1794–1801.
- (139) Friščić, T.; Halasz, I.; Beldon, P. J.; Belenguer, A. M.; Adams, F.; Kimber, S. A. J.; Honkimäki, V.; Dinnebier, R. E. *Nat. Chem.* **2012**, *5* (1), 66–73.
- (140) Abdelhamid, H. N. *TrAC - Trends in Analytical Chemistry*. 2016, pp 122–138.
- (141) Abdelhamid, H. N.; Chen, Z.-Y.; Wu, H.-F. *Anal. Bioanal. Chem.* **2017**, *409* (21), 4943–4950.
- (142) Deng, J.; Wang, K.; Wang, M.; Yu, P.; Mao, L. *J. Am. Chem. Soc.* **2017**, *139* (16), 5877–5882.